Université de Liège
Faculté des sciences
Département de géographie

Modeling of the surface mass balance in Svalbard with the regional climate model MAR over 1958-2010

Mémoire présenté par
Charlotte LANG
en vue de l'obtention de la
maîtrise en sciences géographiques
orientation climatologie

Année académique
2010-2011

Membres du jury
Xavier Fettweis (Promoteur)
Michel Erpicum
Louis François
Aurélia Hubert-Ferrari

Tout d'abord, je tiens à remercier mon promoteur, Xavier Fettweis qui m'a suivie et conseillée pendant un an.

Je remercie également Michel Erpicum de nous avoir poussés pendant 2 ans et de nous avoir appris à être critique.

Merci aussi à Papa et Maman qui m'ont permis de faire ce deuxième master.

Enfin, merci à Whitney, Berny et Modeste pour ces deux super années, sans oublier Amalia, Emilie et Jacques.

Abstract

It is well known that high latitude zones are very sensitive to climate change. As a result of global warming, ice sheet melting has increased which in turn has an influence on climate through modifications of the thermohaline circulation, feedback of ice albedo, sea level rise,...

Svalbard is an archipelago located between 74 and 81°lat N and 60 percent of its area (62 248 km^2) is covered with glaciers and ice sheets. The impact of global warming on the Svalbard cryosphere can be estimated with climate models. However, we need to use regional climate models as they offer the possibility of a higher resolution than general circulation models.

We have carried out a simulation of the Svalbard climate over the last 50 years (from 1958 to 2010) with the regional climate MAR model (tuned for the Greenland ice sheet) at a 10 km resolution forced with the ECMWF reanalysis. As validation, the modeled climate has been compared to near surface measurements at several weather stations through the archipelago. The results show a large interannual variability of the surface mass balance over Svalbard along with an increasing melting. The increase in temperature is responsible for the melting rate and the interannual variability is due to the variations of the mean summer temperature.

List of Figures

List of Tables

Contents

Chapter 1

Introduction

1.1 Historical and geographical context

Svalbard is a Norwegian archipelago located between 74 and 81° lat N and 10 and 35° lon E bordered by the Arctic Ocean to the North, the Greenland Sea to the West, the Norwegian Sea to the South and the Barents Sea to the East. The archipelago, which has a total area of 62 248 km^2 (Liestøl, 1993), is covered by more than 2000 glaciers and ice caps on 59% of its surface. The main islands are Spitsbergen, Nordaustlandet, Edgeøya and Barentsøya (see table 1.1 and figure 1.1).

Figure 1.1: Localization of Svalbard, its main islands and settlements. Source:http://wikitravel.org/shared/Image:Svalbard_topo_map.png

Figure 1.1 shows the topography of the archipelago. Spitsbergen is the most alpine of the islands with a very marked topography going up to 1717 m (Liestøl, 1993) on Newtontoppen (Eastern side of Spitsbergen). On the other hand, Edgeøya, Barentsøya and Nordaustlandet have quite smooth surfaces.

Islands	**Area (km^2)**	**Ice cover (%)**	**Number of glaciers**
Spitsbergen	38612	56.4	1598
Nordaustlandet	15193	74.7	210
Edgeøya	5230	40.7	110
Barentsøya	1321	43.5	126
Kvitøya	710	99.3	1
Prins Karls Forland	622	13.4	33
Kongsøya	195	7.0	30
Svenskøya	140	5.7	20
Bjørnøya	178	0	0
Hopen	47	0	0
Total	62248	58.8	2128

Table 1.1: Svalbard islands (Liestøl, 1993).

The name Svalbard is first mentioned in 1194 in the Sagas of Icelanders, which tell the story of the discovery by Norwegian Vikings of a land they literally called "cold shores". The first irrefutable discovery happened June 10th 1596 when the Dutch navigator Willem Barentsz, searching for the Northeast passage, discovered Bear Island (Bjørnøya), the Southernmost island of the archipelago. On June 17th, the crew reached a new part of the archipelago that Barentsz named Spitsbergen, "pointed mountains", referring to the numerous tops he could see. In 1920, the Treaty relating to Spitsbergen gave Norway sovereignty and delimited the boundaries of the archipelago. It took effect through the Act of 17 July 1925 relating to Svalbard, which changed the name Spitsbergen into Svalbard and set the first Governor of Svalbard. Nowadays, about 2700 persons live on Svalbard. Among them are 2000 Norwegians and a lot of foreign scientists. The capital city, Longyearbyen, hosts the University Centre (UNIS).

1.2 Climate

Svalbard climate is polar-type but is by far warmer than other regions at the same latitude, thanks to the North Atlantic Drift, a branch of the Gulstream. The mean annual temperature is -5/-6°C at Ny-Ålesund weather station and the mean monthly temperature is positive from June to September. Yet, snow can fall at any time in summer and temperatures can be positive even during the winter. Precipitation is quite low on the Western shore of Svalbard (often less than 400 mm) but can be twice as small further

inland (Liestøl, 1993). However, on the mountain tops, precipitation rises due to orographic lifting. The highest amount of precipitation (more than 1000 mm, Liestøl, 1993) is found in the Eastern and Southern parts of the archipelago as the Easterly winds bring humid air from the Barents Sea (Schuler et al., 2007). Moreover, these conditions are very variable in time as Svalbard weather is alternately influenced by dry and cold polar air masses coming from the North and more humid and warm masses from the South (Moholdt et al., 2009).

1.3 Svalbard glaciers and ice caps

Figure 1.2 shows the location of Svalbard glaciers and ice caps.

Figure 1.2: Localization of Svalbard glaciers and ice caps. Source: Liestøl, 1993

Most of Svalbard glaciers are subpolar or polythermal glaciers (Nuth et al., 2010), i.e. glaciers that share both the characteristics of temperate and cold glaciers. In most cases, the temperature of the glacier is close to the melting point in the accumulation area whereas the part of the glacier in the ablation area is frozen to the bed (Liestøl, 1993). However, some very small glaciers (area smaller than 10 km^2) can be considered as polar or cold as their entire mass is far below 0°C (Hagen et al., 2003a).

As a result of their low temperatures, Svalbard glaciers velocities are inferior to 10 m yr^{-1} (Moholdt et al., 2010) and lower than those of temperate glaciers. Indeed, because

of their basal temperature, a thin film of water forms at the base of temperate glaciers. This layer acts as a lubricant and helps the glaciers sliding on the bedrock. Cold glaciers, for their part, are frozen to their bed and their velocities are thus lower.

Moreover, surging type glaciers are frequent in Svalbard (Hamilton and Dowdeswell, 1996). Surging is a cyclic sudden acceleration of the ice flow, 10 to 1000 times faster than usual. In non-surging conditions, the ice flux from the accumulation area of the glaciers to the ablation area maintain a steady longitudinal profile. In surging glaciers, the ice flux is too low compared to the accumulation rate and the slope increases, which also increases the basal shear stress. When the shear stress reaches a critical value, the slope becomes too steep and the ice flow (and thus the velocity of the glacier) rises suddenly. Based on glacier registration, Lefauconnier and Hagen (1991) claim that up to 90 percent of Svalbard glaciers are of the surging type. However, not everybody agrees with this proportion. Indeed, according to Jiskoot et al. (1998) surging type glaciers represent only 13 percent of all the Svalbard glaciers. Svalbard surges are particular for 2 reasons. First of all, the proportion of surging glaciers in Svalbard is huge compared to the mean (less than 1% of the Earth glaciers are of the surging type, according to Murray et al. (2003)). Secondly, during surge episodes, the flow is much slower than elsewhere and a single episode lasts also longer. Murray et al. (2003) stated that this difference is due to a different surge mechanism in Svalbard (thermal influence in the case of Svalbard glaciers).

The most common types of glaciers in Svalbard are small cirque glaciers and valley glaciers, especially in the Western parts of Spitsbergen. In the centre parts of the island, large ice masses divided into streams by mountain ridges are found (Hagen et al., 2003a). The largest one of those ice fields is Olav V Land, located on the Eastern side of Spitsbergen, with an area of about 3000 km^2 (Liestøl, 1993).

On the Eastern islands of the archipelago (Edgeøya, Barentsøya and Nordaustlandet), ice caps are present, as a result of the low topography of these islands. The largest two ice caps are Austfonna (8105 km^2) and Vestfonna (2510 km2) (Dowdeswell et al., 1986) and are located respectively on the Eastern and Western areas of Nordaustlandet. Austfonna has an ice thickness ranging from less than 100 m on the Southeastern coast to 500 m at Austdomen, the top of the island (791 m) and Vestfonna peaks at 630 m.

1.4 Surface mass balance

1.4.1 Definition

Mass balance (MB) is the water (including snow and ice) balance giving the difference between mass gain (accumulation) and loss (ablation). Precipitation contributes to accumulation whereas meltwater runoff, evaporation and sublimation, iceberg calving and basal melting contribute to ablation. Surface mass balance (SMB) is the water balance that takes into account only surface processes (precipitation, runoff, evaporation and sublimation) and can be calculated from the outputs of a regional climate model coupled with a snow model as the MAR model. Modeling dynamical processes such as iceberg

formation requires coupling the climate model with an ice sheet model, which we do not have. That is why we will focus only on the SMB in this thesis.

1.4.2 Mass balance in Svalbard

Mass balance measurements were first carried out in 1950 when the Norsk Polarinstitutt started to measure winter accumulation and summer ablation every two years on Finsterwalderbreen, a small glacier in the South of Spitsbergen. In 1966 and 1967, observations started at Austre Brøggerbreen and Midre Lovénbreen, two glaciers a few kilometers away from Ny-Ålesund weather station. Figure 1.2 shows the location of these glaciers. Results showed negative mass balance almost every year, suggesting that ablation is greater than accumulation and thus that the Svalbard glaciers/ice sheets are losing mass. (Hagen and Liestol, 1990; Hagen, 1993). The measurements were made by direct measurements of accumulation and ablation: snow depth and density measurements in snow pits and stake readings . Unfortunately, this method is very time consuming and thus only a few glaciers mass balance have been investigated with this method, most of them over short time series. Moreover, only a few of them were made on glacier larger than 10 km^2 and they were almost all located on the Western and central parts of Spitsbergen. Greuell et al. (2007) list all the 14 glaciers on which such measurements have been made.

Less information is available for larger glaciers with higher altitude accumulation area, which are thought to be closer to the equilibrium (Hagen, 1996). Pinglot et al. (1999) determined the surface mass balance of some higher altitude glaciers and two ice caps from 1986 up to 1997 based on ice-cores showing the reference layers from Chernobyl (1986) and the atmospheric nuclear tests in Novaya Zemlya (maximum in 1961-1962). Their results showed positive balances with no general trend.

Moreover, extensive measurements only began a few years ago. For example, Moholdt et al. (2010) measured elevation changes from 2003 to 2008 based on measurements made by the satellite ICESat (see chapter 4 for comparison). Bamber et al. (2005) estimated elevation changes between 1996 and 2002 of 12 glaciers and 6 ice caps located on Spitsbergen and Western Nordaustlandet using lasers aboard planes flying at 400 m of altitude. Their results indicate a general thinning (with a maximum thinning rate in South Spitsbergen) except for the highest altitudes in Northeastern Spitsbergen. They also showed that the thinning rate was higher between 1996 and 2002 than for the 30-40 last years.

The results also show differences in the mass balance according to the altitude (Hagen and Listøl, 1990, Moholdt et al, 2009). Indeed, the balance is negative near sea level and becomes positive if the altitude is high enough. The altitude where the balance is zero is called the equilibrium line altitude (ELA) and varies with the location. Hagen et al. (2003b) modeled its distribution throughout Svalbard and their results showed values of 200 to 700 m above sea level, with lower values on the Southeastern side than on the Western side due to the precipitation pattern.

Several authors have also worked on the reconstruction of past mass balance based on observations made at Brøggerbreen, Lovénbreen and Kongsvegen since the sixties. Lefau-

connier and Hagen (1990) reconstructed the mass balance of Brøggerbreen back to 1912 using correlations between the measured mass balance and climatic parameters measured at Ny-Ålesund weather station. The best results were obtained using the positive degree day methodology from July to September for the summer balance and precipitation from October to May for the winter balance. Their reconstructions results showed that Brøggerbreen started to shrink around 1918, which was in agreement with pictures taken at that time. Rasmussen and Kohler (2007) performed reconstructions since 1948 using a model running with meteorological data from NCEP/NCAR reanalysis (wind and relative humidity at the 850 hPa level for the winter balance and mean temperature at 500 m from June to August for the summer balance). Their cumulative curves showed an increase in the mass loss between the periods 1948-1967 and 1968-2005 because of an increase in the summer balance due to the rise in summer temperatures. Unfortunately, their study is based on the huge resolution reanalysis output, which cannot reflect the local conditions of the Svalbard topography. Finally, Flemming et al. (1997) used an energy balance model (EBM) to model the SMB and evaluate the impacts of climate change on its evolution. Their results showed a diminution of 0.61 mm y^{-1} (mm water equivalent) per degree of rising temperature and a growth of 90 m $°C^{-1}$ for the ELA.

1.5 Regional climate models and the MAR model

Regional climate models (RCM) are climate models that, unlike global models (GCM, General Circulation Model), can be run over only a part of the planet and offer several advantages compared to those GCMs. Firstly, working with a global model is time consuming and their resolution needs to be coarse. Regional climate models on the other hand, can be run with a much higher spatial and temporal resolution, which allow to get results for areas too small to be modeled with GCMs. Indeed, the typical resolution for the atmospheric module of a GCM is a few degrees of latitude/longitude and Svalbard is represented in the GCMs by only 4-5 pixels at best, which is clearly insufficient compared to the scale of the modeled processes. Furthermore, the GCMs are tuned to produce the best results under our latitudes and neglect polar zones while the physics used in the RCM can be calibrated over the studied area. In addition, they can represent the topography more precisely and hence take into account more local effects of it. In contrast, regional models need to be forced at their boundaries, either with a GCM or, like in our case, reanalysis, which are outputs of a global model forced with actual data.

The MAR model (for Modèle Atmosphérique Régional) is a RCM developed at first for polar regions (Gallée and Schayes, 1994).

The model consists of an atmospheric module that solves the primitive equations of fluid dynamics (horizontal conservation of momentum, hydrostatic equilibrium, continuity for compressible fluid and energy) in a system where the normalized pressure is the vertical coordinate (sigma coordinates):

$$\sigma = (p - p_t)/(p_s - p_t)$$

where p is the pressure at the considered level, p_s is the surface pressure and p_t, at the top of the atmosphere. In that coordinate system, the different layers have therefore different thickness, the layers closer to the surface being thinner than higher ones. This system is well suited for meteorological, oceanographic and climatological applications.

The hydrological cycle (Gallée, 1995) includes a conservation equation for specific humidity and a cloud micro-physical model containing conservation equations for cloud droplets, cloud ice crystals, raindrops and snowflakes.

The atmospheric model is coupled with a surface model called SISVAT (Soil Ice Snow Vegetation Atmosphere Transfer) (De Ridder and Gallée, 1998, Gallée, Guyomarc'h and Brun, 2001) through the exchange of radiative fluxes (short and long wave), latent and sensible heat, momentum, precipitation,... This model is a vertical 1D multi-layered model consisting of a soil-vegetation module, a snow/ice energy balance module resolving most of the processes occurring at the surface of the snow/ice pack and based on the CROCUS model from the CEN (Centre d'Etudes de la Neige). The soil-vegetation module simulates the exchanges of heat and moisture with the atmosphere above the land without snow or ice while the snow/ice module deals with the exchanges between the atmosphere and the sea-ice, the glaciers and ice sheets and the snow covering the land. Snow layers are described in the snow metamorphism module of the snow/ice module by their temperature, density, height, age, liquid water content, dendricity and sphericity of the crystals and grain size. The energy balance between the soil and the snow is computed in the thermodynamic module of the snow/ice module through the absorbed shortwave flux, the longwave fluxes (upward and downward), the sensible and latent heat fluxes at the surface, the melting and sublimation of snow/ice and evaporation and refreezing of the meltwater heat fluxes, the heat fluxes due to precipitation (solid and liquid), condensation and deposition and the heat flux from the ground.

Finally, the reanalysis based 6 hourly forcings are temperature, humidity and wind at each vertical level, surface pressure and sea surface temperature (SST) and sea ice cover (SIC) above the ocean.

1.6 Objective and relevance of the work

The main goal of this work is the modeling of the surface mass balance of Svalbard with the regional climate model MAR over 1958-2010. We have carried out a simulation of the Svalbard climate over the last 50 years with the MAR model (tuned for the Greenland ice sheet) at a 10 km resolution forced with the ECMWF reanalysis. As validation, the modeled climate has been compared to near surface measurements at several weather stations through the archipelago. Finally, we have investigated the time evolution of the surface mass balance and its relation to the Svalbard climate.

Modeling the mass balance is of great interest in the context of the global warming. Indeed, high latitude zones are very sensitive to climate changes and a warming as projected currently should cause an acceleration of the ice sheets melting which in turn has an influence on climate through modifications of the thermohaline circulation, feedback

of ice albedo, sea level rise,...

Climate models and, in this case, mass balance study are suitable tools for evaluating the impact of global warming on the cryosphere and Svalbard appears to be an appropriate area for such a work. Moreover, its position at the end of the North Atlantic Drift and its relatively mild climate make it even more sensitive to global warming.

Knowing the importance of the high latitudes zones and the prognostic use of those models by the IPCC, it appears that properly modeling the polar climates and the processes related to it is needed.

Chapter 2

Simulations and set up

2.1 Creation of the ice-land-sea mask

The first step of this work was to produce a 10-kilometer resolution topography, which is done by NESTOR, MAR pre-processor, from the topography coming from GTOPO30 (Global 30 Arc-Second Elevation), a global digital elevation model (DEM) with a horizontal resolution of 30 arc seconds (corresponding more or less to one kilometer). If we compare our topography (figure 2.1) to figure 2.2, we see that it is too low in many places. Indeed, the maximum of elevation reaches 1000 meters while Newtontoppen peaks at more than 1700 meters (blue dot in figure 2.2).

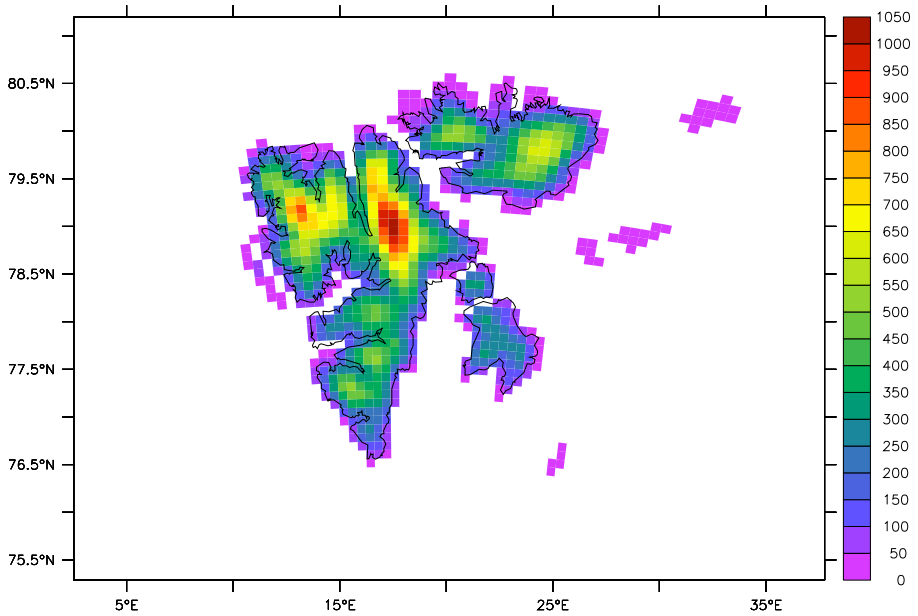

Figure 2.1: Topography (m) created by the MAR model.

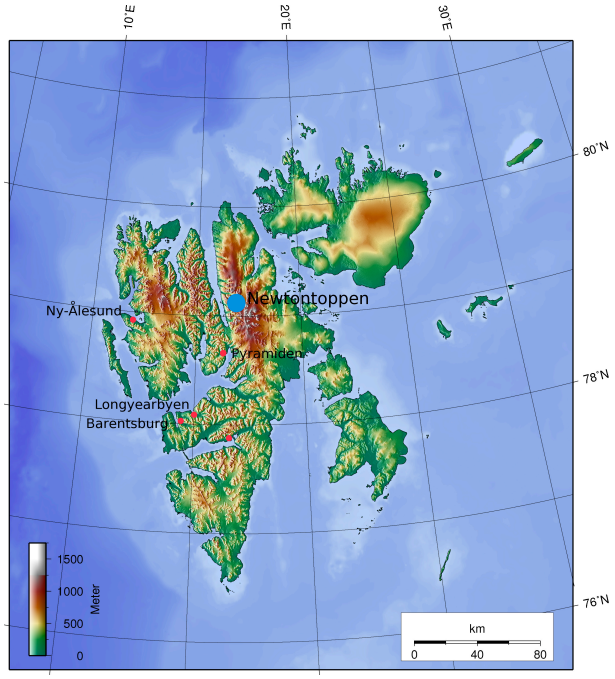

Figure 2.2: Topography of Svalbard. The blue dot represents the location of Newtontoppen. Source: http://commons.wikimedia.org/wiki/File:Svalbard-topo.png

This is partly due to the fact that the 10 km resolution is not able to represent the sharp topography of Svalbard and of Spitsbergen in particular. But the difference is not only due to the resolution. Indeed, Austfonna is an ice cap with gentle slopes and its maximum elevation is also underestimated here (about 600 m in our topography and 800 m in reality (Moholdt et al., 2009)). Therefore, a more precise DEM is needed and the MAR model should ideally be run at a higher resolution. However, increasing the resolution by a factor 2 requires at least 8 times more computation time. A factor 4 comes from the fact that multiplying the resolution by 2 leads to 4 times more pixels and another factor 2 is needed to satisfy the Courant-Friedrichs-Lewy condition saying that the time step has also to be divided by 2 in order to ensure the stability of the simulation. If this was not done, the model would jump from pixel i-1 to pixel i+1 during time step Δt without calculating anything on pixel i.

These biases in the GTOPO30 based 10 km topography impact the simulated precipitation as the amount of precipitation due to orographic lifting will be underestimated. This impacts also the temperature which could be too high here.

Then, an ice-land-sea mask (needed for the MAR snow model) has been created over the topography using maps showing the presence of glaciers and ice caps over Svalbard and is shown in figure 2.3. The ice pixels have been added manually over the land-sea mask created by NESTOR from the GTOPO30-based topography.

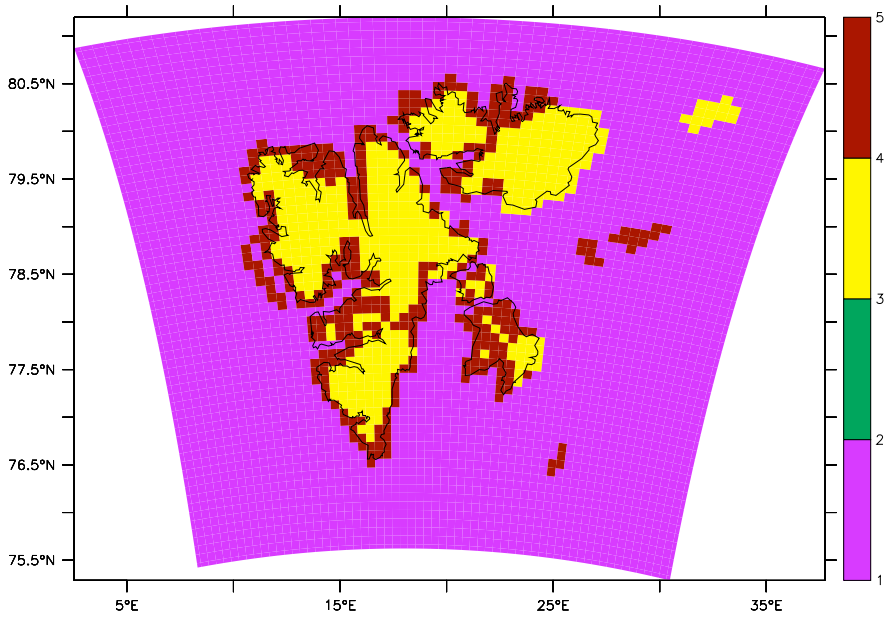

Figure 2.3: Ice-land-sea mask created by NESTOR. Pink: sea, red: land, yellow: ice.

2.2 Choice of the domain

We then had to choose the most suitable size for the spatial domain and the location of Svalbard in the domain, the first part being done by looking at the simulated precipitation. Indeed, if the domain is too small, the model will not produce enough precipitation because precipitation is not forced at the boundaries of the domain but is produced by the cloud scheme using specific humidity as forcing. Therefore 10 pixels at least far away from the boundaries are needed before MAR being able to simulate precipitation. On the other hand, a too large domain will uselessly require a too long computation time.

We chose the location of the archipelago in the domain by looking at the dominant circulation pattern direction. Indeed, let us assume that the surface pressure pattern is the same the whole year long. As a consequence, the dominant winds (bringing with them moist air from the sea, which produces precipitation) come from the same direction whatever the time of the year is, Southwest for example. In this case, we should have placed Svalbard in the upper right corner of the domain as there would not be much precipitation coming from the Northeastern side and thus no need for a lot of pixels on this side.

In our case, the monthly long term sea level pressure mean patterns computed by the NCEP/NCAR reanalysis showed two dominant directions according to whether it is the summer or the winter (see figure 2.4) and we chose to place Svalbard in the middle of the domain.

We then chose the size of the domain by comparing the simulated amount of precipitation over each domain for 2 months of the years 2009 that were representative of the

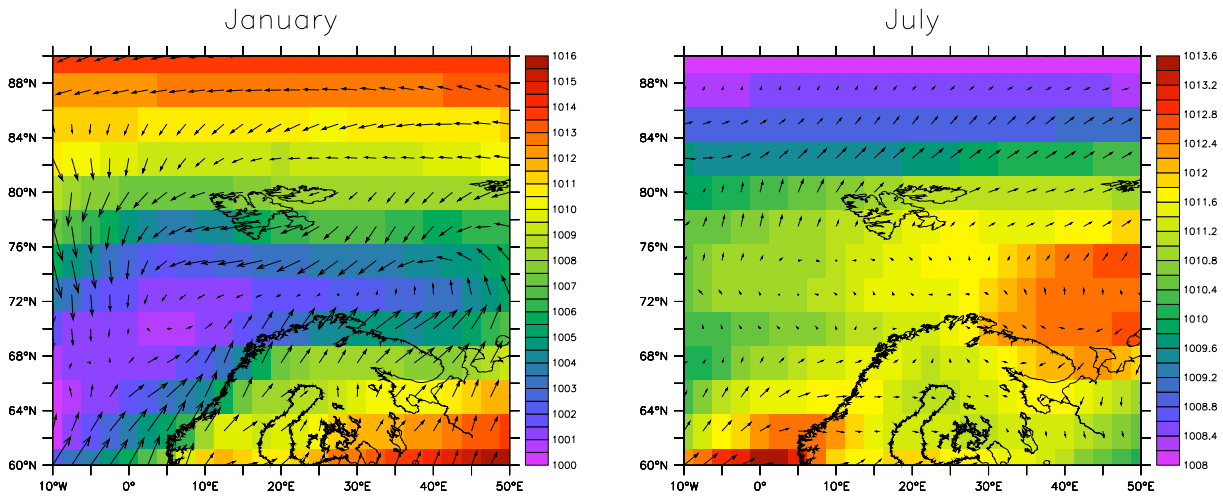

Figure 2.4: Long term monthly mean surface pressure in January (left) and July (right) and wind direction (vectors). Note that the scale is not the same Source:http://www.esrl.noaa.gov/psd/data/reanalysis/reanalysis.shtml

mean circulation pattern, i.e. February and September. Table 2.2 summarizes the size of the domains.

Domain	**A**	**B**	**C**	**D**	**E**
Size (pixels)	75X85	80X90	85X95	90X100	100X110

Table 2.1: Size of the different domains in pixels (10X10 km).

Figures 2.5 to 2.8 show the difference of simulated precipitation over domains A to D in percent with respect to domain E (the largest one) and table 2.2 lists this difference in percent, averaged only over the land pixels, along with the calculation time needed in percent of the calculation time required in domain E.

As seen from tables 2.1 and 2.2 and figures 2.5 to 2.8, domain C is a good compromise between computation time and the amount of precipitation modeled. Therefore, we decided here to work with domain C.

Note that we computed the precipitation only from the sixth day of the month (i.e for a period of 23 days in February and 25 days in September) in order to remove the impact of the spin up time of the atmosphere in this case.

2.3 Simulations

We have run the MAR model over a 85X95 pixels domain, at a spatial resolution of 10 kilometers between 1958 and 2010. The boundaries were forced every 6 hours by the

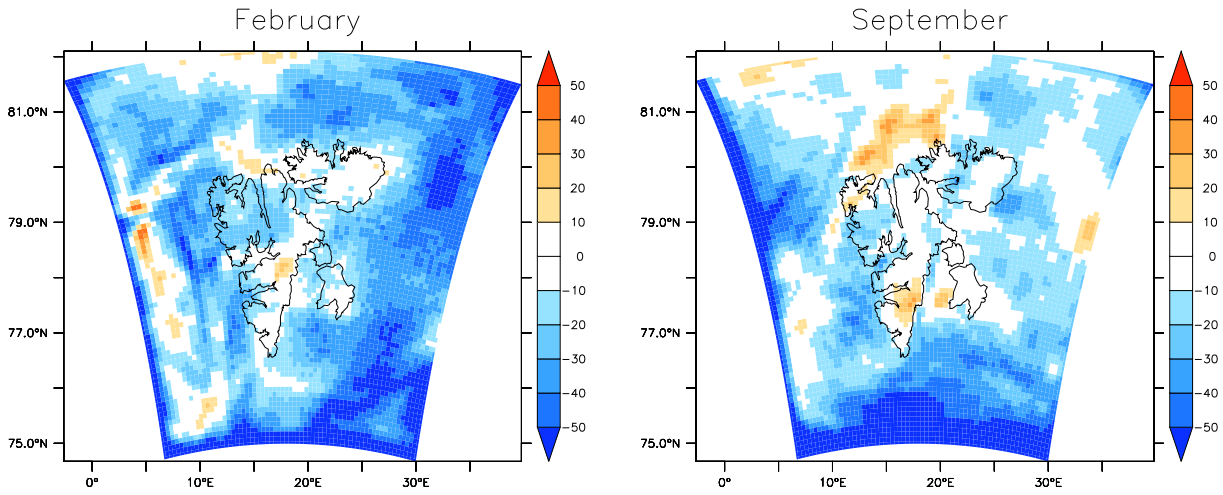

Figure 2.5: Precipitation difference (%) of domain A with respect to domain E.

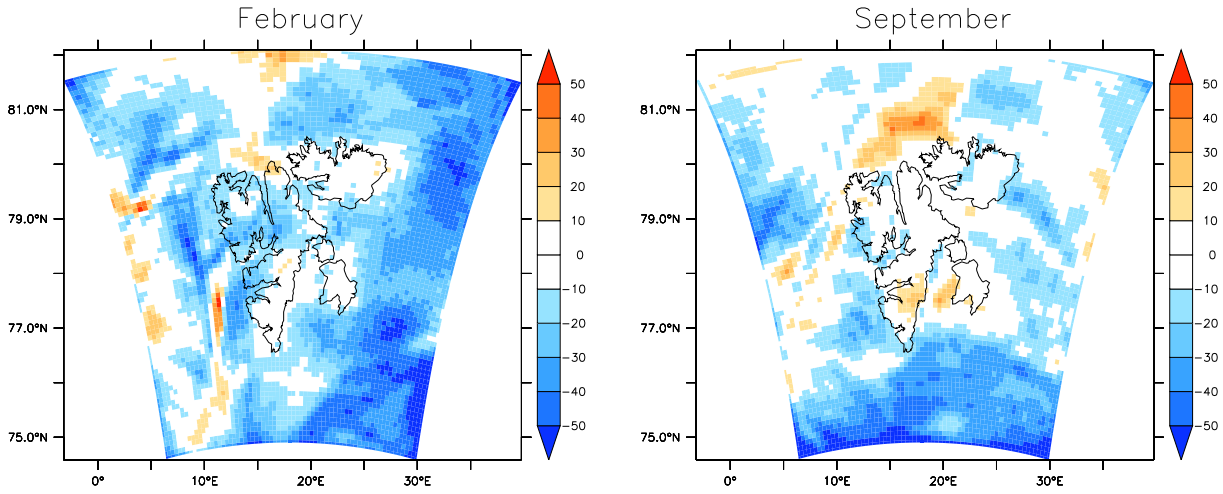

Figure 2.6: Precipitation difference (%) of domain B with respect to domain E.

Domain	**A**	**B**	**C**	**D**
February	-12.13	-11.04	-8.65	-5.78
September	-6.26	-2.18	1.02	2.49
Time	57.95	65.45	73.41	81.82

Table 2.2: Difference of precipitation (%) over domains A to D with respect to domain E. Computing time (Time (%)) needed for each domain with respect to the computing time needed for domain E (=100%).

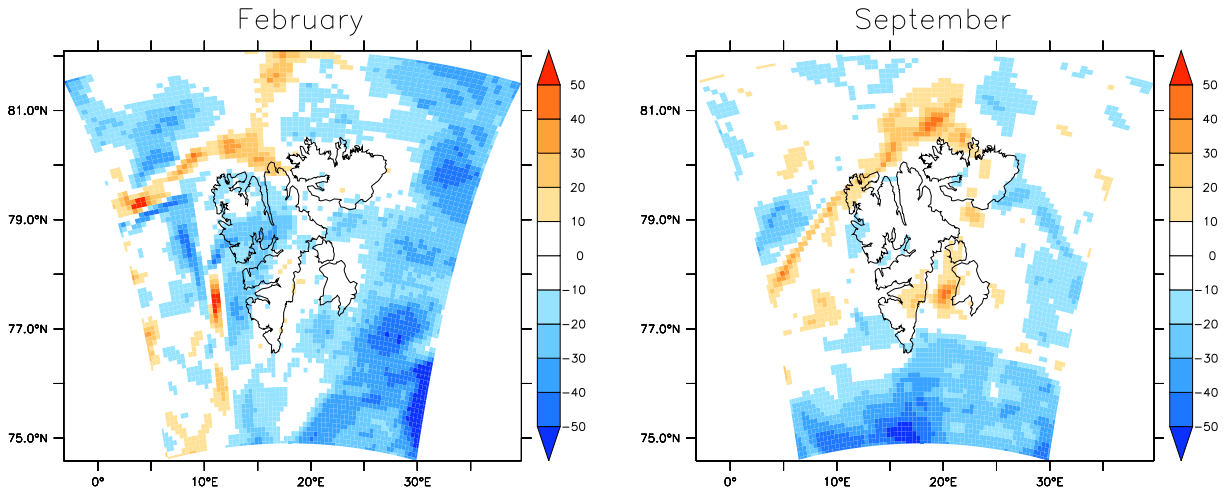

Figure 2.7: Precipitation difference (%) of domain C with respect to domain E.

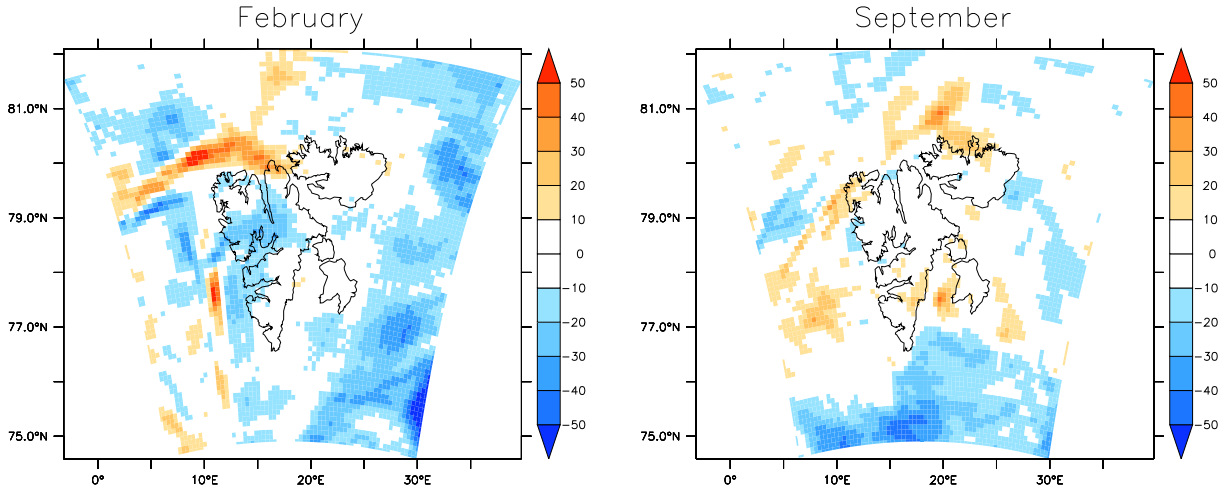

Figure 2.8: Precipitation difference (%) of domain D with respect to domain E.

ECMWF (European Centre for Medium-range Weather Forecast) reanalysis: ERA-40 from 1958 to 1999 and ERA-INTERIM from 2000 to 2010. The spin-up time was two years. The spin-up time is the time the model has to be run before the results are correct enough to be used. In our case, we ran 53 simulations (one for each year from 1958 to 2010 on one CPU) of three years each: the year (YYYY) used as final result and the two previous years (YYYY-1 and YYYY-2) as spin-up. Each of simulation started at the end of summer (the 1st of September) of YYYY-3 and the ice sheet pixels were initialized with 9 meters of ice and one meter of snow. Two meters were added during the simulation when the thickness was less than 8 meters as a result of the melting. Knowing that MAR is not parallelized, the strategy of starting 53 simulations over 53 CPUs for simulating 53 years allows to gain computation time.

Our outputs were annual NetCDF files containing daily mean for each pixel. Those we used were: mean near surface (3 meters, i.e the first vertical level height of the model) temperature and wind, total amount of precipitation (rainfall and snowfall), mean surface pressure, runoff, sublimation and evaporation and surface mass balance.

Chapter 3

Validation of the MAR model

To validate the MAR model over Svalbard, we compared the results of the model to near surface measurements from the Norwegian Meteorological Institute (www.eklima.met.no). On one hand, we collected daily measurements of surface temperature, surface pressure, wind speed and precipitation at several stations located throughout the archipelago and shown in figure 3.1.

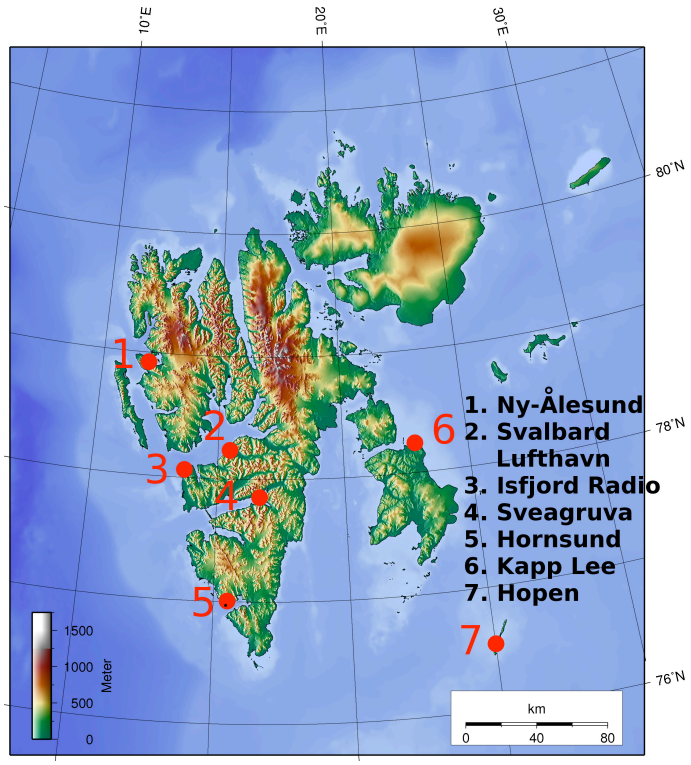

Figure 3.1: Localization of the weather stations used for validation. Source:http://commons.wikimedia.org/wiki/File:Svalbard-topo.png

On the other hand, we selected the corresponding daily data from the model outputs for the 10kmX10km pixel the nearest to the location of the station. Table 3.1 gives the station coordinates and elevation and the coordinates and elevation of the corresponding pixel in the MAR model.

Station	Latitude (°N)	Longitude (°E)	Latitude MAR (°N)	Longitude MAR (°E)	Elevation (m)	Elevation MAR (m)
Ny-Ålesund I	78.93	11.93	78.87	11	42	24.22
Ny-Ålesund II	78.92	11.93	78.87	11	8	24.22
Svalbard Lufthavn	78.25	14.47	78.22	15.36	28	189.60
Isfjord Radio	78.07	13.63	78.02	13.66	7	60.42
Sveagruva	77.88	16.72	77.86	15.43	9	138.60
Hornsund	77.00	15.50	76.96	15.21	10	41.46
Kapp Heuglin	78.25	22.82	78.19	22.84	14	66.57
Hopen	76.51	25.01	76.52	24.96	6	0.44

Table 3.1: Weather stations used for validation. Station coordinates, coordinates of the corresponding pixel in the MAR model, elevation of the station, elevation of the pixel in the MAR model. Weather stations data source: www.eklima.met.no

In some cases, the corresponding pixel was covered by ice or its altitude was much higher than that of the one from the station because the resolution of the model could not resolve the sharp topography near the sea shore. In this case, we preferred to choose a more distant pixel that would better represent the climate of the station. That is why there is sometimes up to one degree longitude difference (about 20 km here) between the station location and the pixel. However, for Svalbard Lufthavn and Sveagruva stations, there is still a difference in altitude of more than 100 m, which will influence the comparison of the modeled variables versus observations.

For each station, we calculated, for temperature, pressure and wind velocity, the mean annual from both observed and modeled values, averaged over the whole observation period, as well as the bias, the root mean square error and the correlation between both time series. Here, the biases are the difference between the modeled values and the observed ones. For precipitation, we computed the mean total observed and modeled amounts, the mean difference and the correlation between both times series. If there were too many missing data or outliers, the corresponding years were not considered in the calculations. The second column of tables 3.2 to 3.7 lists the chosen years.

Note that Ny-Ålesund weather station changed location in 1974. As there was no overlap in the data (the time series ended in July 1974 for the first station and began in august 1974 for the second one), we could not compare their data and we chose to treat them as two separate data sets called *Ny-Ålesund I* and *Ny-Ålesund II* hereafter. As we performed our calculations only over full years of observations, we selected the years 1969 to 1973 for the first station and 1974 to 2010 for the second one and did not use the data collected during the year 1974.

Finally, some of the time series were very short, with less than 5 years of measurements (Ny-Ålesund I, Hornsund and Kapp Heuglin). Nevertheless, we decided to keep them in tables 3.2 to 3.7 as they were showing the same type of results as the other time series.

3.1 Temperature validation

3.1.1 Mean annual temperature

Table 3.2 summarizes near-surface temperature comparison. In Sveagruva, the years 2003 and 2004 contained some outliers. The temperature suddenly dropped for a few days and neither the model nor the other stations reproduced it. In Hornsund, more than one third of the data was missing for the year 2008 and only the years 2007 and 2008 were almost complete in Kapp Heuglin.

Station	Years	Number years	Observed T (°C)	Modelled T (°C)	RMSE (°C)	Bias (°C)	R^2
Ny-Ålesund I	1969-1973	5	-6.03	-9.05	4.62	-3.02	0.91
Ny-Ålesund II	1975-2010	36	-5.29	-7.83	3.71	-2.54	0.92
Svalbard Lufthavn	1976-2010	35	-5.29	-9.49	5.05	-4.2	0.93
Isfjord Radio	1958-1975	18	-5.05	-9.00	5.44	-3.95	0.91
Sveagruva	1979-2002	30	-5.97	-9.99	5.04	-4.02	0.93
	2005-2010						
Hornsund	2006-2007	4	-2.49	-6.20	4.85	-3.71	0.93
	2009-2010						
Kapp Heuglin	2007-2008	2	-6.13	-9.43	4.7	-3.3	0.9
Hopen	1958-2010	53	-5.51	-7.41	4.12	-1.9	0.89

Table 3.2: Temperature validation. Biases are the difference between modeled and observed temperature.

From table 3.2 we see that the correlation between the model and the observations is very good. Indeed, the determination coefficient R^2 is greater than 0.90 for every station but one. The model is hence able to simulate very well the variability of the observations.

However, there is a systematic bias, the modeled temperature being lower than the observations by about 2 to 4 degrees. At Sveagruva and Svalbard Lufthavn stations, the difference in altitude between the station and the corresponding pixel in the MAR model is about 150 meters, which probably enhances the difference between the modeled and observed temperatures. This negative bias has an influence on the modeled surface mass balance. Indeed, on the one hand, a lower temperature than expected should reduce the melting during the summer months. On the other hand, a decrease in temperature induce an underestimation of the amount of precipitation because colder air contains less moisture than warmer air and then produces less precipitation. This induces a too

low amount of snowfall that contributes to accumulation during the winter, but also less rainfall which could increase the melting during the summer.

Figure 3.2 shows, as example, the mean observed and modeled temperature at Svalbard Lufthavn station for the year 1986.

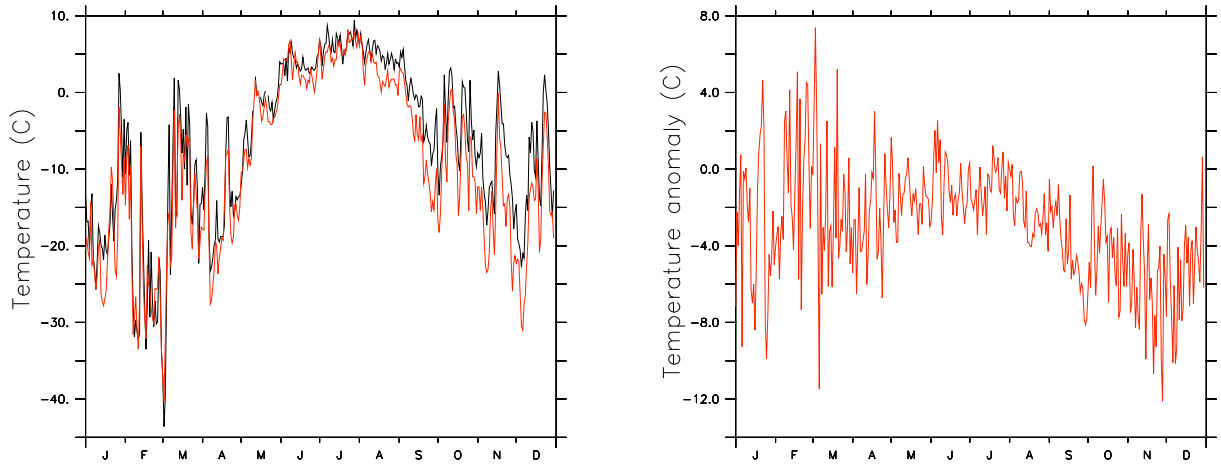

Figure 3.2: Left: Daily evolution of the mean temperature measured at Svalbard Lufthavn during the year 1986 (black curve) and modeled mean temperature for the corresponding pixel (red curve). Right: Mean temperature anomaly. The anomaly is the difference between the modeled and the observed temperature.

3.1.2 Seasonal mean temperature

As we will see in chapter 5, summer temperature has a greater influence on the surface mass balance than mean annual temperature. Indeed, interannual variability of the SMB is mainly driven by the variability of the melting, which is highly correlated to the summer temperature. That is why we also considered separately mean summer temperature (June, July and August mean) and mean winter temperature (December, January, February) during this validation.

Tables 3.3 and 3.4 show that the correlation between modeled and observed temperature is still good for winter (R^2 >0.8, except for Ny-Ålesund II and Kapp Heuglin stations, which have short time series) but that the daily variability of the observed mean summer temperature is less well simulated by the MAR model (R^2 drops to 0.5). However, the "cold" bias is reduced for the summer temperature. The model is less than 1 degree colder than the observations in summer, except for Sveagruva and Svalbard Lufthavn. But again, part of the difference for these stations is due to the altitude difference between the station and the corresponding pixel. In contrast, the bias rises up to 7 degrees in winter. The effect of a too low summer temperature on runoff is therefore moderate but the wintry effect of the precipitation is increased.

Station	Years	Number years	Observed T (°C)	Modelled T (°C)	RMSE (°C)	Bias (°C)	R^2
Ny-Ålesund I	1969-1973	5	3.68	2.94	1.95	-0.74	0.60
Ny-Ålesund II	1975-2010	36	3.91	3.10	1.92	-0.81	0.59
Svalbard Lufthavn	1976-2010	35	4.81	2.55	2.81	-2.26	0.70
Isfjord Radio	1958-1975	18	3.49	3.12	1.76	-0.37	0.55
Sveagruva	1980-2001	28	4.74	2.71	2.55	-2.04	0.68
	2005-2010						
Hornsund	2006-2007	4	3.70	3.06	1.61	-0.65	0.47
	2009-2010						
Happ Heuglin	2007-2008	2	1.50	1.22	1.53	-0.28	0.56
Hopen	1958-2004	52	1.73	2.75	1.90	1.02	0.51
	2006-2010						

Table 3.3: Summer temperature (JJA) validation. Biases are the difference between modeled and observed temperature.

Station	Years	Number years	Observed T (°C)	Modelled T (°C)	RMSE (°C)	Bias (°C)	R^2
Ny-Ålesund I	1969-1973	4	-11.94	-17.24	6.48	-5.3	0.78
Ny-Ålesund II	1975-2010	35	-12.2	-15.74	4.6	-3.54	0.85
Svalbard Lufthavn	1976-2010	34	-12.94	-18.35	6.16	-5.41	0.87
Isfjord Radio	1958-1975	17	-11.69	-18.55	7.67	-6.86	0.81
Sveagruva	1979-2010	31	-14.27	-19.27	5.98	-5.01	0.86
Hornsund	2005-2010	5	-6.07	-12.11	6.7	-6.04	0.87
Kapp Heuglin	2006-2008	2	-10.4	-16.38	6.91	-5.99	0.73
Hopen	1958-2004	51	-12.16	-16.86	6.25	-4.7	0.82
	2005-2010						

Table 3.4: Winter temperature (DJF) validation. Biases are the difference between modeled and observed temperature.

This difference in the bias is due to the fact that the MAR model simulates too little longwave radiation. In winter, the amount of solar radiation is lower than in the summer and is even nil in December and January as the sun never rises and the longwave radiation is thus the major source of energy in the radiative transfer equation. In the summer, on the other hand, the contribution of the shortwave radiation lowers the bias. This effect is enhanced by the overestimation of shortwave radiation by the MAR model. The same biases have been highlighted over the Greenland ice sheet by Fettweis et al. (2011).

Notice that the chosen years can be different for the "annual", the summer and the winter validation. Indeed, in some cases, almost a whole month of observations was missing. In this case, the missing values would not have a huge impact on the annual statistics but could be more significant for the seasonal ones. We thus chose to keep these observations in the annual validation but to reject it from the corresponding seasonal one.

3.2 Surface pressure validation

Station	Years	Number years	Observed SP (hPa)	Modelled SP (hPa)	RMSE (hPa)	Bias (hPa)	R^2
Ny-Ålesund I	1969-1973	5	1004.07	1007.31	3.54	3.24	0.98
Ny-Ålesund II	1975-2010	36	1008.47	1006.95	1.97	-1.52	0.99
Svalbard Lufthavn	1976-2010	35	1006.09	986.09	20.04	-20.01	0.99
Isfjord radio	1958-1975	18	1008.86	1003.25	5.8	-5.61	0.98
Sveagruva	1979-2010	32	1008.82	992.6	16.3	-16.22	0.98
Kapp Heuglin	2007-2008	2	1007.11	1000.19	7.45	-6.92	0.96
Hopen	1958-2010	53	1008.27	1009.92	2.09	1.65	0.99

Table 3.5: Surface pressure validation. Biases are the difference between modeled and observed surface pressure.

As we can see from table 3.5, the correlation between the model and the observations is excellent for the surface pressure. Biases are mainly due to the difference in altitude between the station and the pixel in the MAR model. The reason why surface pressure is so well represented by the model is that the pressure variability depends mainly on the large scale circulation coming in MAR from the reanalysis-based boundaries forcing. Knowing that the reanalysis are notably constrained by the actual observed surface pressure at Svalbard, this explains why the observed pressure variability compares very well with the reanalysis and then with the MAR model. Temperature, on the contrary, is a more local process (i.e. more independent of the boundaries forcing) and then more complicated to model. Figure 3.3 shows the evolution of the surface pressure at the second station in Ny-Ålesund for the year 2003.

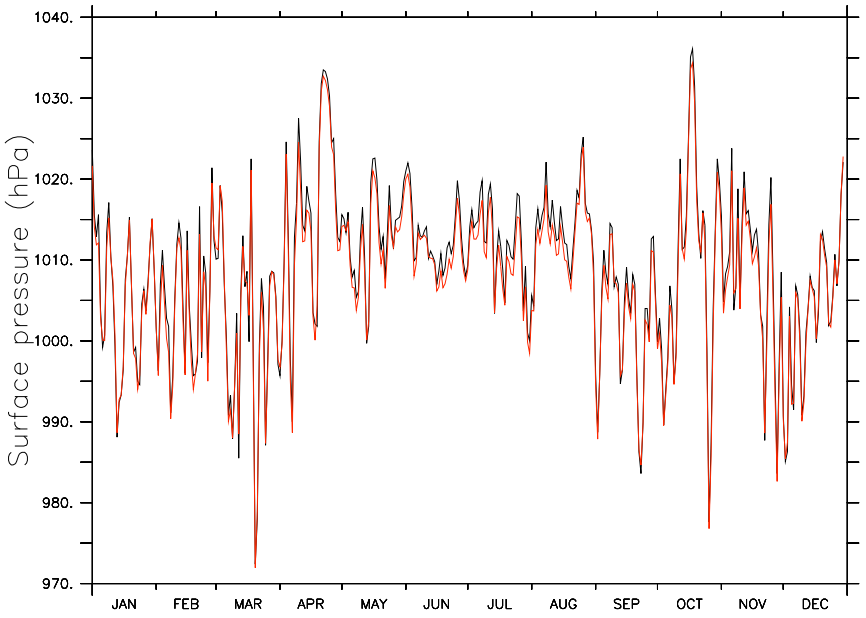

Figure 3.3: Daily evolution of the surface pressure measured at Ny-Ålesund (second station) during the year 2003 (black curve) and modeled surface pressure for the corresponding pixel (red curve).

3.3 Wind validation

Here, the correlation is less good but the average values are nevertheless quite correct (see table 3.6). There is no general sign in the biases, for some stations the MAR models higher values of the wind speed than observed, for the other ones lower values. This is due to the fact that wind depends on very local conditions that cannot be modeled with a 10-kilometer resolution.

3.4 Precipitation validation

There was no precipitation data for Kapp Heuglin and for Sveagruva after 2002. For the other stations, a lot of data was often missing as shown in figure 3.5.

This time, the model is not able to represent the observed variability of precipitation. Moreover, the modeled total annual amount of precipitation is often less than the half of the observed amount. There are several reasons to this difference. First of all, it is known that the current used version of the MAR model underestimates the precipitation over Greenland (Fettweis, 2011). Then, we use the topography coming from the GTOPO30 digital elevation model, which appears not to be able to represent the Svalbard topography very well. For example, the highest top, Newtontoppen, is more than 1700 m high but the maximum altitude in our 10kmX10km grid is about 1000 m. Besides, the 10-km resolution plays also a role in the bad representation of the Svalbard topography. Indeed,

Station	Years	Number years	Observed wind (m/s)	Modelled wind (m/s)	RMSE (m/s)	Bias (m/s)	R^2
Ny-Ålesund I	1969-1973	5	4.16	4.41	2.67	0.25	0.37
Ny-Ålesund II	1975-2010	36	3.64	4.44	2.64	0.8	0.39
Svalbard Lufthavn	1976-2010	35	4.94	5.2	2.69	0.26	0.4
Isfjord Radio	1958-1975	18	7.98	4.98	4.07	-3	0.49
Sveagruva	1979-2000	31	4.9	4.49	2.27	-0.41	0.51
	2002-2010						
Hornsund	2005-2010	6	5.81	5.73	1.99	-0.08	0.69
Kapp Heuglin	2007-2008	2	5.25	4.35	2.27	-0.9	0.55
Hopen	1958-2010	53	5.24	5.04	2.21	-0.2	0.5

Table 3.6: Wind speed validation. Biases are the difference between modeled and observed wind speed.

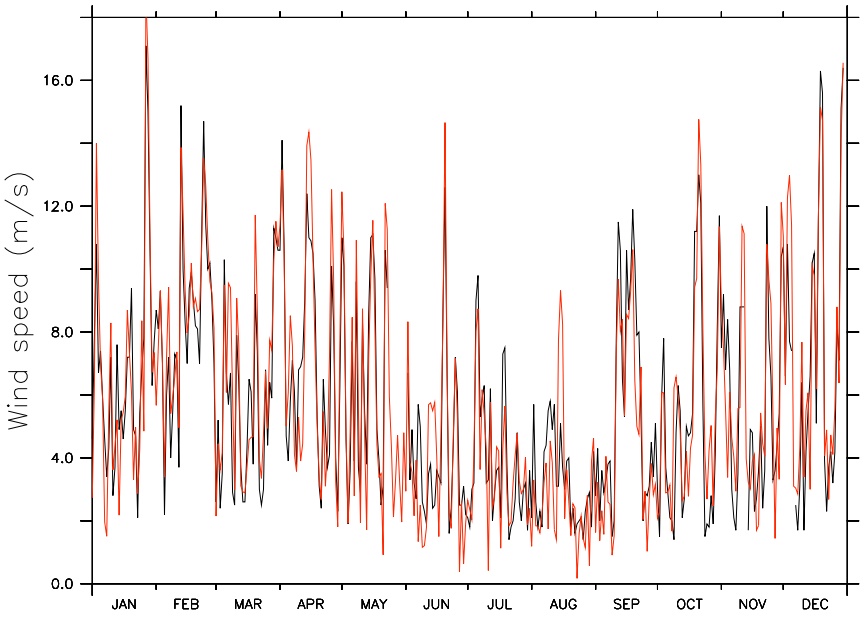

Figure 3.4: Daily evolution of the wind speed measured at Hornsund during the year 2010 (black curve) and modeled wind speed for the corresponding pixel (red curve).

Station	Years	Number years	Observed P (mm)	Modelled P (mm)	Difference (mm)	R^2
Ny-Ålesund I	1969-1973	5	338.78	132.03	-206.75	0.04
Ny-Ålesund II	1975-2010	36	403.46	128.4	-275.06	0.03
Svalbard Lufthavn	1976-2010	35	188.01	196.48	8.47	0.05
Isfjord Radio	1958-1975	18	468.63	149.72	-319.91	0.05
Sveagruva	1979-2002	24	264.51	192.96	-71.55	0.07
Hornsund	2005-2009	5	484.44	193.81	-290.63	0.02
Hopen	1958-2010	53	417.69	209.3	-208.38	0.06

Table 3.7: Precipitation validation. The sixth column gives the difference between the mean total annual modeled amount of precipitation and the observed one.

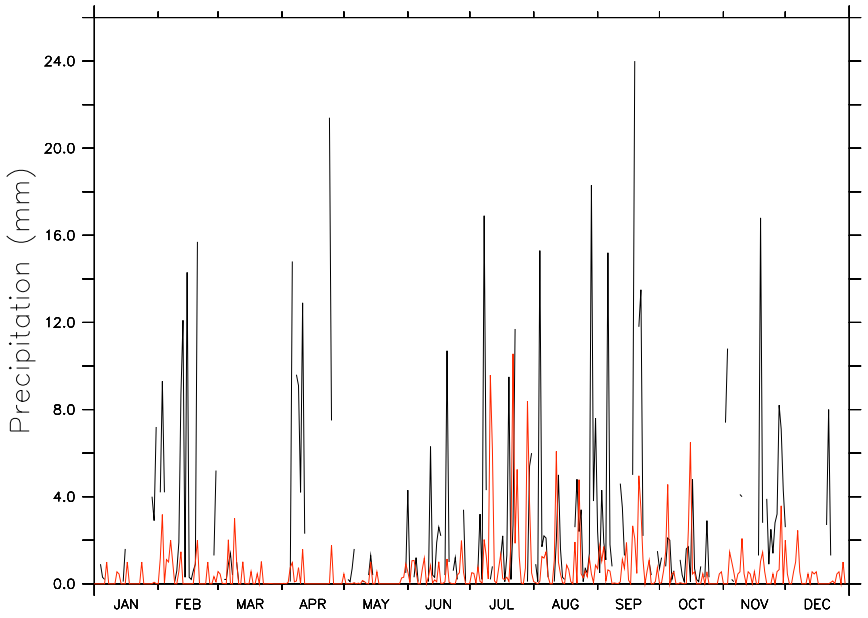

Figure 3.5: Daily evolution of the precipitation measured at Isfjord Radio during the year 1967 (black curve) and modeled precipitation for the corresponding pixel (red curve).

the land relief is very marked and 10 km is not enough for representing it precisely. As a consequence, precipitation due to oragraphic lifting is reduced. Unfortunately, we do not have any observed data in the mountainous regions to corroborate this. Thirdly, we should not run the model with a resolution of 10 kilometers and 100-kilometer resolution forcings in one step. Instead, we should perform an intermediate run with a lower resolution then use its outputs to force the boundaries of the 10-km resolution run.

Finally, as we already mentioned it, the lower temperature impacts the amount of precipitation.

This will result in biases in the modeled surface mass balance.

3.5 Conclusion

We have shown that the MAR model is too cold over Svalbard and simulates too few precipitation. This problem could be in part solved by using a more precise DEM and increasing the spatial resolution.

Furthermore, the only data we could get came from stations located along the coast and, for most of them, on the Western side of Spitsbergen. The only two stations outside this main island are Kapp Heuglin and Hopen and have either very short time series (or no measurements at all in the case of precipitation) or are located on a 4-kilometer wide island, which is less than our spatial resolution. We can not either compare our results with other models as this is the first time that a regional climate model is run over Svalbard. As a consequence, we could not confirm nor invalidate the model behavior outside the Western coastal area.

Chapter 4

Results: surface mass balance

4.1 Spatial distributions

4.1.1 Surface mass balance

Figure 4.1 shows the mean annual surface mass balance computed from 1958 to 2010 along with the isolines of altitude.

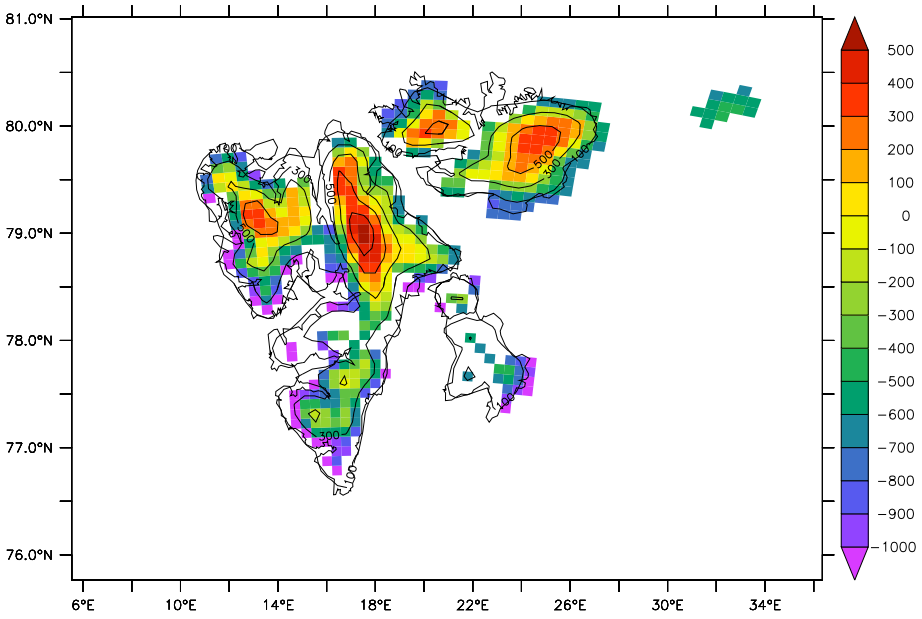

Figure 4.1: Mean annual surface mass balance (mm) over 1958 - 2010 for each pixel of the domain covered with ice and isolines of altitude (represented every 200 m).

We can see that, at low altitude, near the coast, the surface mass balance is negative, meaning that ice is lost every year in average. At higher altitude, however, the balance is positive and the glaciers and ice caps gain mass. The altitude at which the balance

goes from negative to positive varies according to the location in the archipelago. On Austfonna and Vestfonna, it is about 300 to 400 meters. According to Schuler et al. (2007), we should find that this altitude is lower on the Southeastern side of Austfonna because of the winds from the Barents Sea bringing more precipitation. Unfortunately, the resolution is too coarse to allow us to detect any difference. On the Northeastern part of Spitsbergen, this altitude is 400-500 meters and rises up to 600 meters on Northwestern Spitsbergen.

In table 4.1, we give the mean annual surface balance for the 7 different zones defined by Moholdt et al. (2010) and shown in figure 4.2.

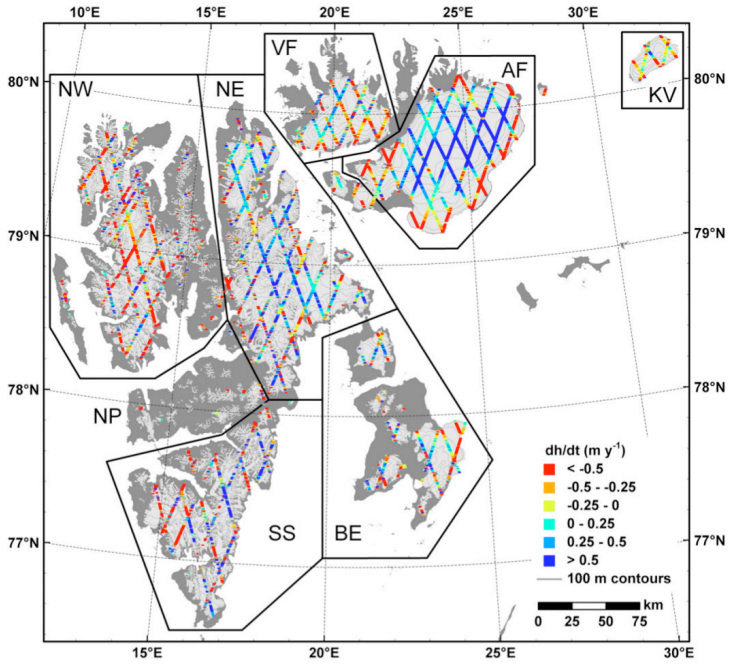

Figure 4.2: Location of the 7 zones defined by Moholdt et al. (2010). NW = Nortwestern Spitsbergen, NE = NorthEastern Spitsbergen, SS = South Spitsbergen, NP = Nordenskiöld peninsula, BE = Barentsoya and Edgeoya, VF = Vestfonna, AF = Austfonna, KV= Kvitøya.

For each of these regions, the surface mass balance is negative in the MAR model, meaning that, even in zones with high accumulation areas, the accumulation driven gain can not compensate the melt-induced loss.

Zone	SMB (mm)
Austfonna	-231.64
Vestfonna	-270.47
Northwestern Spitsbergen	-361.44
Northeastern Spitsbergen	-206.16
Southern Spitsbergen	-635.22
Barentsøya/Edgeøya	-751.85
Kvitøya	-551.69
Total Svalbard	-358.00

Table 4.1: Mean annual surface mass balance (mm) for each zone defined by Moholdt et al. (2010).

4.1.2 Components of the surface mass balance

Precipitation

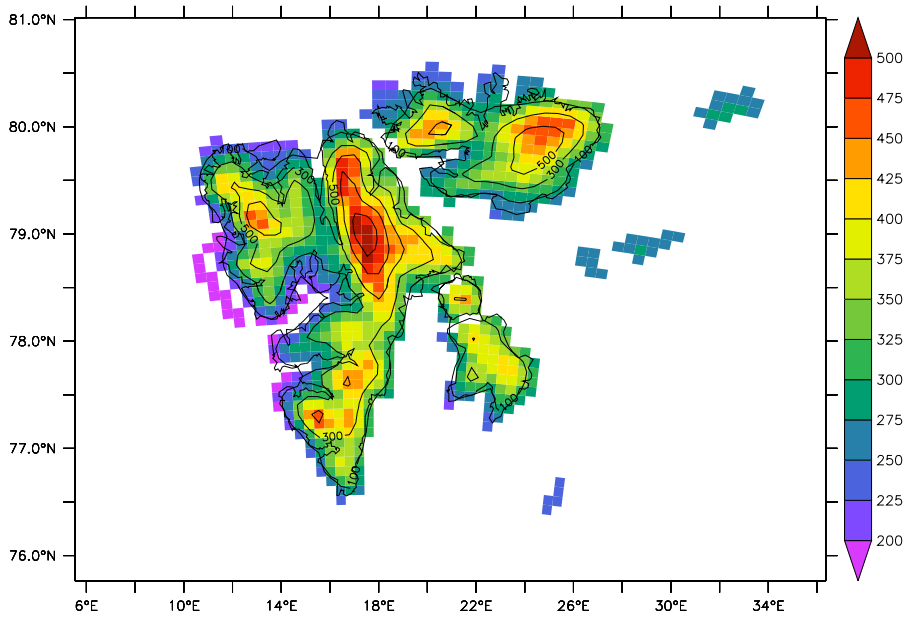

Figure 4.3: Annual total amount of precipitation (solid and liquid) (mm) averaged over 1958-2010.

First of all, figure 4.3 shows that the amount of precipitation is lower on the Western coast of Spitsbergen than on the Eastern side. The Western coast is also the location of the minimum of precipitation (less than 250 mm). This is due to the more humid winds coming from the Barents Sea, i.e from the East (Schuler et al. 2007). Then, we also see in the precipitation pattern the variation of the topography, as the amount of

precipitation rises up to more than 500 mm when the altitude gets higher. Secondly, this result corroborate those we found in the validation section (chapter 3): the amount of precipitation simulated by the MAR model is too low. Indeed, according to Liestøl (1993), precipitation is about 400 mm on the Western coast and more than 1000 mm in the Southeastern part of Spitsbergen, where the winds bring humid air on the mountain slopes. In our case, the highest amount of precipitation is found in Newtontoppen region (Northeastern Spitsbergen) instead of Southern Spitsbergen and is twice as small as the real maximum.

Runoff

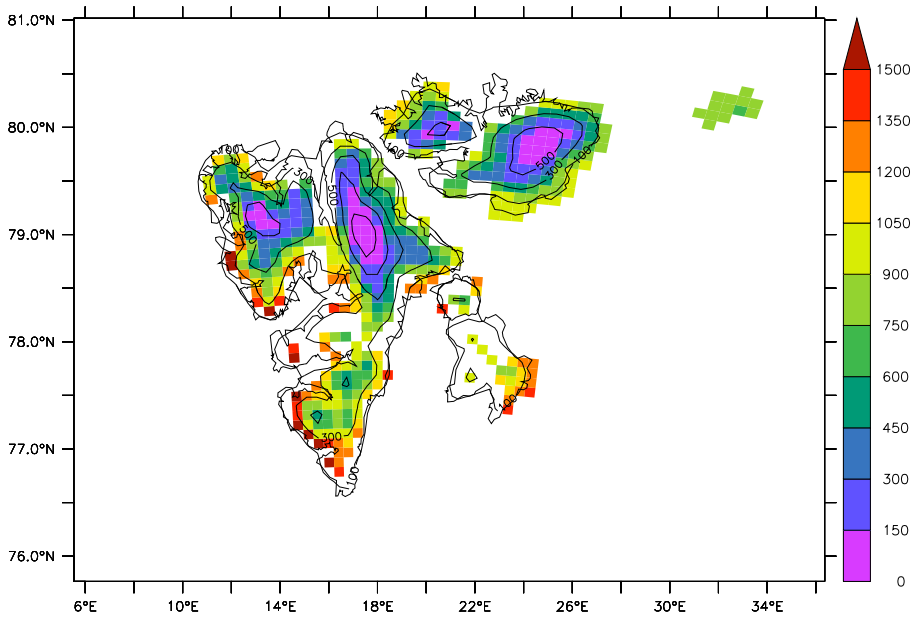

Figure 4.4: Annual total runoff (mm) averaged over 1958-2010.

Figure 4.4 shows what will be confirmed later: runoff is the most important component of the surface mass balance. As a matter of fact, runoff and surface mass balance patterns are the same (but in the opposite direction). The surface mass balance is low where the amount of runoff is high and vice versa.

Sublimation and evaporation

Figure 4.5 shows that the highest areas have the more negative sublimation and evaporation. A negative value means that deposition (condensation of water vapor) is higher than sublimation and evaporation. Hence, at higher altitudes, more vapor condensate as it is colder.

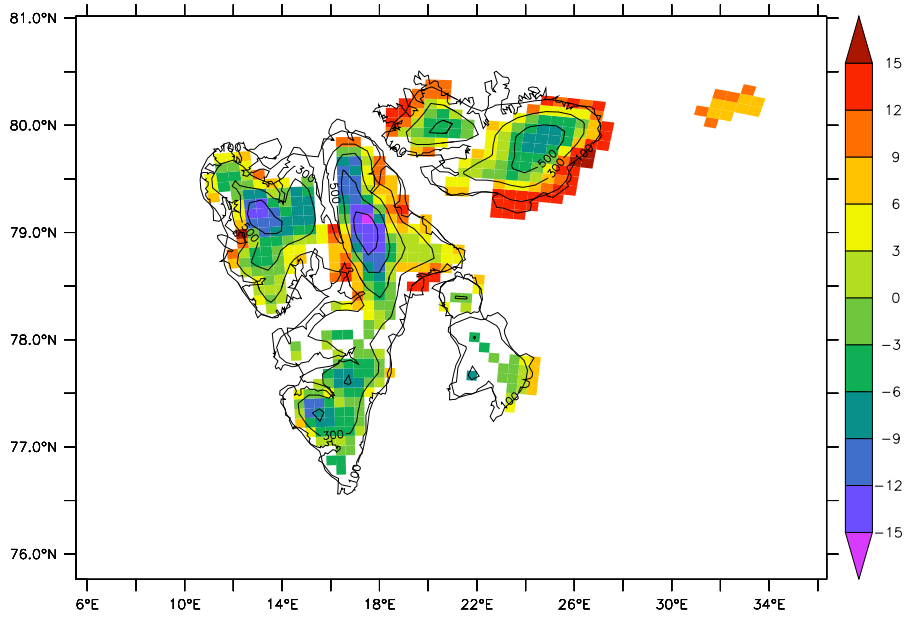

Figure 4.5: Annual total sublimation and evaporation (mm) averaged over 1958-2010.

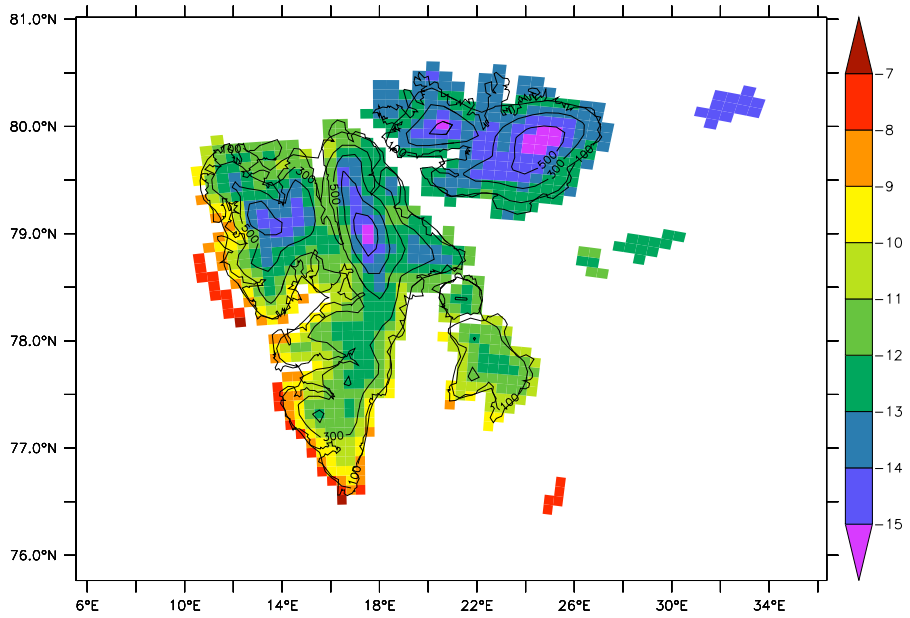

Figure 4.6: Mean annual temperature (°C) averaged over 1958-2010.

4.1.3 Temperature

Again, as for precipitation, the spatial gradient reflect the change in altitude (figure 4.6), temperatures lower than -15°C are found in the center parts of Austfonna and Vestfonna and on the highest regions of Northeastern Spitsbergen while they drop to -7 to -12°C at lower altitude. Meanwhile, there is a West-to-East gradient showing the effect of the North Atlantic Drift bringing warmth on the West coast of the archipelago.

4.2 Temporal evolution and trends

4.2.1 Evolution

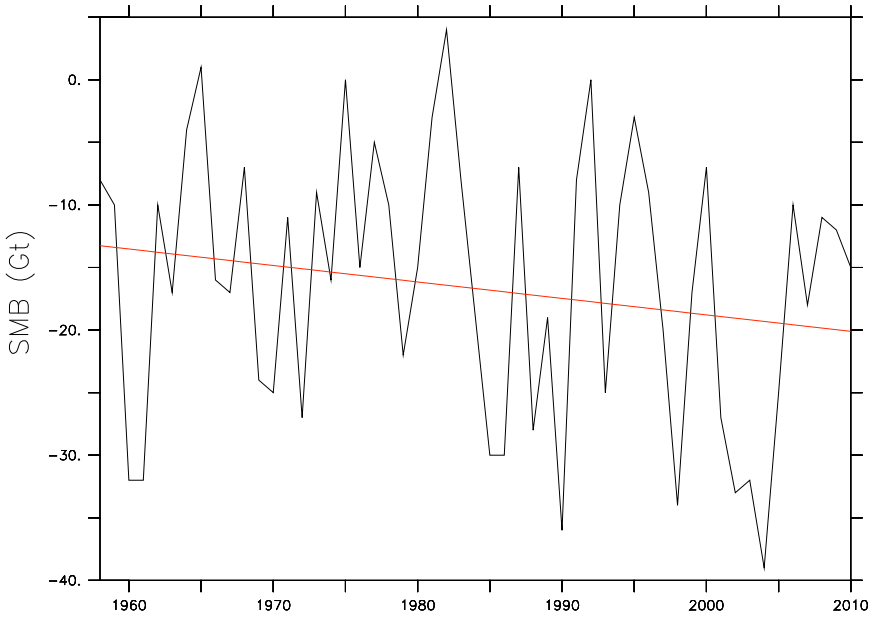

Figure 4.7: Evolution of the total (summed over all the pixels) annual surface mass balance (black curve) and trend (red curve) over 1958-2010.

In figure 4.7, we have plotted the annual evolution of the surface mass balance summed over all the pixels covered with ice. Surface mass balance shows a great year-to-year variability along with a general decrease (see section 4.2.2 for the trends).

The 4 years with the highest balance are 1965, 1975, 1982 and 1992. These years correspond to an amount of runoff lower than average (see table 4.2). As we will see in chapter 5, runoff mostly determines the surface mass balance variability. The precipitation varies much less.

Furthermore, these four years do not all have especially low mean summer temperature (see table 4.3). Indeed, in 1975, the mean summer temperature was even significantly higher than the mean. While in chapter 5 we will establish that mean summer temperature

Year	SMB (Gt)	Runoff (Gt)	Precipitation (Gt)
1965	1.27	12.64	14.11
1975	0.5	19.73	20.36
1982	4.82	12.47	17.41
1992	0.09	19.35	19.5
Mean	-16.68	33.57	16.95
SD	10.79	10.49	2.81

Table 4.2: Surface mass balance, runoff and precipitation of the highest surface mass balance years. SD = standard deviation.

mainly determine the amount of runoff, the amount of snowfall during the winter has also an influence on the summer runoff. Indeed, if snow is present, meltwater will percolate through it and there will be less runoff than above bare ice. Moreover, as the albedo of the snow (0.65-0.85) is higher than that the one of the ice (0.4-0.5), there will be less melt above snow than above ice. If a lot of snow has fallen the previous winter, the bare ice will appear later and there will be less runoff.

Year	RU anomaly (Gt)	T anomaly (°C)	SF anomaly (Gt)
1965	-21.13	-0.48	0.24
1975	-14.04	0.56	4.43
1982	-21.3	-0.24	0.41
1992	-14.42	0.14	5.7
SD	10.83	0.51	2.7

Table 4.3: Runoff (RU), mean summer temperature (T) and snowfall (SF) anomalies with respect to the mean. Snowfall are taken from September to May. As we need the snowfall from September the year before, we could not calculate this amount for the year 1958. Standard deviations (SD) are therefore calculated between 1959 and 2010.

Indeed, in 1975, there has been more snowfall than average (see table 4.3). In 1992, the temperature was also slightly higher than the mean summer temperature (although it is not significant) and the snowfall was significantly higher than average.

Table 4.4 lists the surface mass balance, the runoff and the precipitation for the 4 lowest SMB years. The runoff values are significantly higher than average for the 4 years and are among the highest values. Precipitation is significantly lower for two years (1998 and 2002). The year 1972 has the third highest value of runoff (50.73 Gt) but is even not in the most negative surface mass balance top ten (-27.61Gt) due to is very high amount of precipitation (23.01 Gt, second position).

Moreover, we observed an increase of the surface mass balance, after meeting the lowest

Year	SMB (Gt)	Runoff (Gt)	Precipitation (Gt)
1990	-36.56	57.18	20.46
1998	-34.37	47.98	13.54
2002	-33.49	46.84	13.4
2004	-39.09	56.13	16.94
Mean	-16.68	33.77	17.05
SD	10.79	10.88	2.82

Table 4.4: Surface mass balance, runoff and precipitation for the lowest surface mass balance years. SD = standard deviation.

value in 2004 (-39.09 Gt). This is consistent with the results of Moholdt et al. (2010) contrary to Greenland where melting was particularly high these last years (Fettweis et al., 2010). Indeed, circulation over Greenland brought air from the South while in Svalbard, the air was coming from the opposite direction, i.e. it was cold and dry polar air.

Finally, we have investigated the evolution of the surface mass balance for the 7 zones defined by Moholdt et al. (2010). Figure 4.8 shows this evolution from 1958 to 2010 and table 4.5 gives the determination coefficients between the different time series.

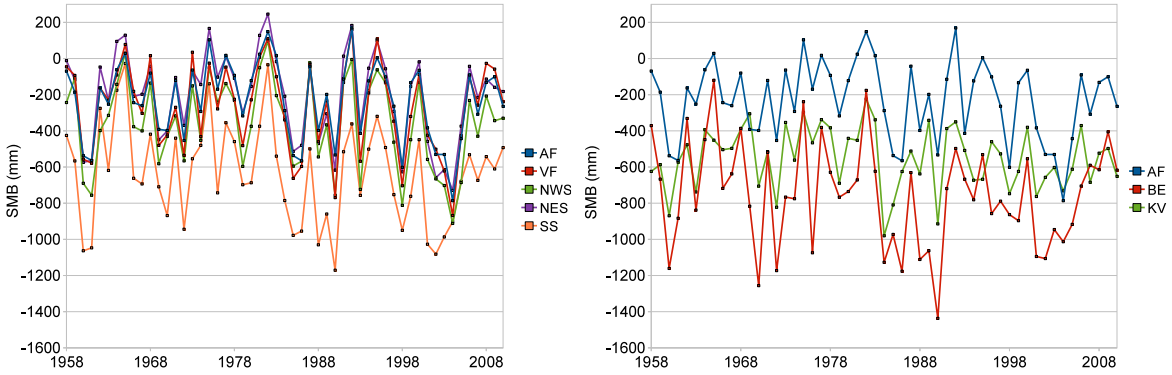

Figure 4.8: Evolution of the surface mass balance over 1958-2010 for the 7 zones defined by Moholdt et al. (2010). AF: Austfonna, VF: VEstfonna, NWS: Northwestern Spitsbergen, NES: Northeastern Spitsbergen, SS: Southern Spitsbergen and BE: Barentsøya and Edgeøya, KV: Kvitøya. Austfonna time series is also shown on the second figure for comparison.

Firstly, we can see that Austfonna, Vestfonna, Northwestern Spitsbergen and Northeastern Spitsbergen (four of the five Northern zones with Kvitøya) have the same behavior, as indicated by the values of the determination coefficients. South Spitsbergen surface

AF	1						
VF	0.9	1					
NW	0.88	0.9	1				
NE	0.93	0.87	0.89	1			
SS	0.73	0.7	0.7	0.85	1		
BE	0.55	0.56	0.44	0.59	0.79	1	
KV	0.47	0.41	0.36	0.4	0.42	0.42	1
	AF	**VF**	**NW**	**NE**	**SS**	**BE**	**KV**

Table 4.5: Determination coefficients between the time series of surface mass balance for the 7 zones between 1958 and 2010. NW = Nortwestern Spitsbergen, NE = NorthEastern Spitsbergen, SS = South Spitsbergen, BE = Barentsoya and Edgeoya, VF = Vestfonna, AF = Austfonna, KV= Kvitøya.

mass balance is a little bit less correlated to the previous four series and the values are often lower than for the four other zones. On the other hand, Barentsøya and Edgeøya and Kvitøya have their own proper behavior and their surface mass balance evolution is much less correlated to the other series.

The reason why Northern Spitsbergen has a lower surface mass balance than the three other Northern zones is that, due to the spatial resolution, the MAR model can not resolve the complex topography of the Northwestern and Northeastern zones and the altitude is lower than it is in reality. As Austfonna and Vestfonna are located on plateau regions, the topography is better represented. Therefore, there will be more melting on Northwestern and Northeastern Spitsbergen than expected. However, the surface mass balance is still higher on Northeastern than on Northwestern Spitsbergen because of the difference in altitude of these two zones.

Figure 4.9 shows the interannual variability of the mean summer temperature between 1958 and 2010 (average = -0.86°C, standard deviation = 0.5°C).

Finally, precipitation varies much less than runoff (Standard deviation = 2.81 Gt for precipitation and 10.49 Gt for runoff, see figure 4.10) and is often lower than runoff. Therefore, runoff variability will mainly determine the surface mass balance interannual variability (see chapter 5). For their part, sublimation and evaporation contribute very few to the surface mass balance, with a maximum contribution of 3.19 Gt in 1968 and varies also less than precipitation (SD = 1.09 Gt)

4.2.2 Trends

We have performed linear regressions analysis in order to determine the trend of the evolution of the surface mass balance, its components and the mean summer temperature. We have fitted equations of the type A= a+b×t to the different time series (A_i, t_i),

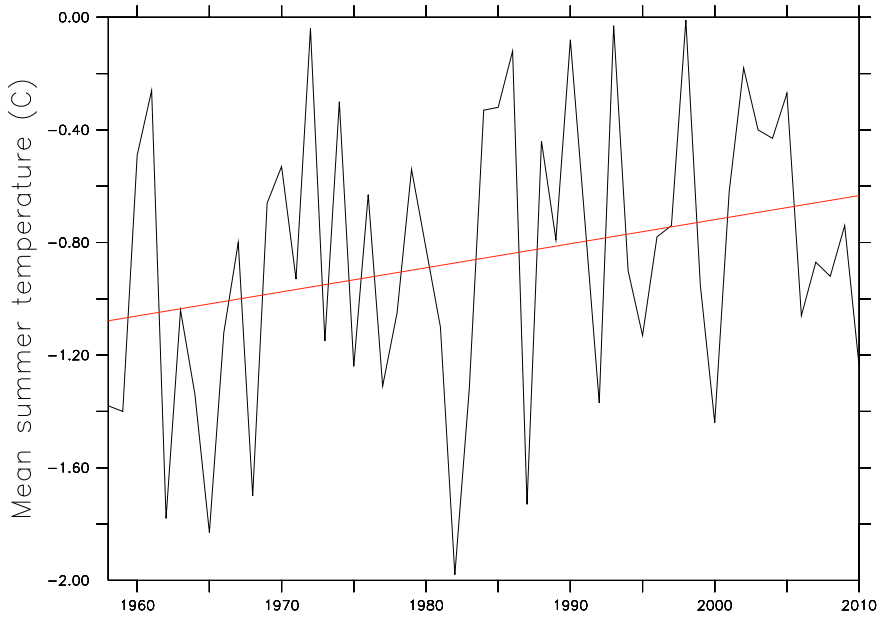

Figure 4.9: Evolution of the mean summer temperature (black curve) and trend (red curve) over 1958-2010.

where A_i represents the value of the variable (SMB, precipitation, runoff, sublimation and evaporation and mean summer temperature in our case) for the year t_i.

Then, we have evaluated if those trends were significant or not by calculating the uncertainty range associated to it. The following formulas give the uncertainty range for the 95% confidence interval (Snedecor and Cochran, 1971):

$$\begin{cases} e_1 = \sum(\text{trend}(a_i) - a_i)^2 \\ e_2 = \sum(t_i - \text{mean}(t_i))^2 \\ \text{range} = \sqrt{e_1/((2010 - 1958 - 1) \times e_2)} \times k \end{cases}$$

where

- t_i is the i^{th} year of the time series
- a_i is the value of the variable for the year t_i
- trend(a_i) is the value of the trend for the year t_i
- k=1.96 for the 95% level of confidence

The trend is significant if its value is higher than the uncertainty range.

Table 4.6 gives, for surface mass balance, its components and mean summer temperature, the regression equation, the trend and its uncertainty range. Figures 4.7, 4.9 and 4.11 illustrate it.

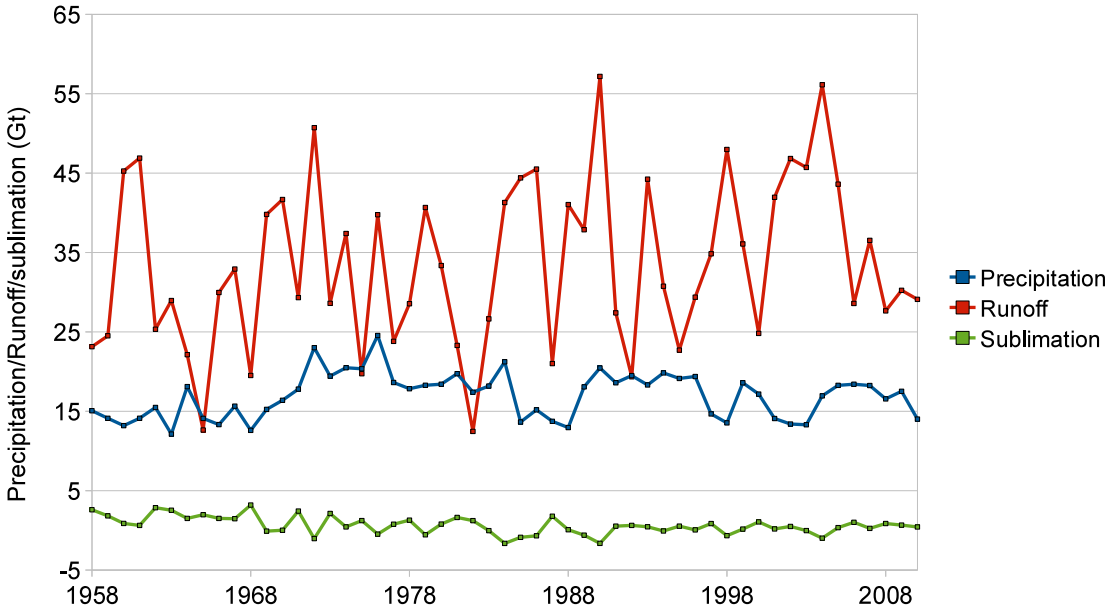

Figure 4.10: Evolution of the total annual amount of precipitation (blue curve), runoff (red curve) and sublimation and evaporation (green curve) over 1958-2010.

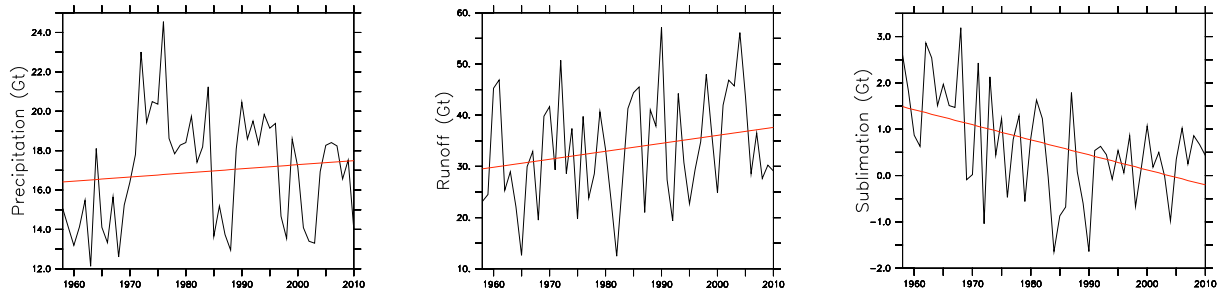

Figure 4.11: Evolution of the total precipitation (left), runoff (middle) and sublimation and evaporation (right) (black curves) and their trends (red curves) over 1958-2010.

Variable	Regression equation	Trend	Uncertainty
SMB	SMB = -13.13-0.13 t	-0.13	0.19
Runoff	RU = 29.36+0.16 t	0.15	0.18
Precipitation	P = 16.39+0.02 t	0.020	0.050
Sublimation and evaporation	SU = 1.52-0.0325 t	-0.032	0.017
Mean summer temperature	T = -1.09+0.0086 t	0.0084	0.0087

Table 4.6: Linear regression equation, trend and uncertainty range on the trend for surface mass balance, runoff, precipitation, sublimation and evaporation and mean summer temperature. The confidence interval is 95%. Trends and uncertainty ranges are in Gt yr^{-1} for SMB, runoff, precipitation and sublimation and evaporation and in $^{\circ}$ yr^{-1} for temperature

From table 4.6 and the figures we see that the surface mass balance is decreasing while the runoff, the amount of precipitation, sublimation and evaporation and the mean summer temperature are increasing. However, none of those trends are significant, except for sublimation and evaporation.

4.3 Comparison with the literature

Finally, we have compared the results of the MAR model to the literature to validate once more the model. Long surface mass balance series are available for Austre Brøggerbreen, Midtre Lovénbreen and Finsterwalderbreen (see, for example Hagen and Liestøl, 1990). However, those glaciers have a small area: about 5 km^2 for Brøggerbreen and Lovénbreen and 35 km^2 for Finsterwalderbreen. Polish and Russian teams have also computed mass balance time series on Hansbreen (since 1989) and Vøringbreen (since 1966) but again, these glaciers are too small to be modeled with our 10-kilometer resolution. Therefore, we can unfortunately not compare the evolution of their surface mass balance to the results of the MAR model.

Some extensive measurements campaigns began recently. We have thus compared our results to those of Moholdt et al. (2010). They have estimated mean annual and seasonal elevation changes from October 2003 to March 2008 from laser altimetry measurements by ICESat, a NASA satellite dedicated to measure, between others, heights and ice sheet mass balance. Their measurements took place during 35-day campaigns in October/November for the winter balance and in February/March for the summer balance. As a consequence, we could not determine a precise date for the beginning and end of the winter and summer seasons and fixed the beginning of the summer season to March 1st and the winter season to November 1st, as it should more or less correspond to the middle of the campaigns.

Figures 4.12 and 4.13 show our annual and seasonal average results and tables 4.7 and 4.8 compare our results to those of Moholdt et al. Figure 4.12 also compares the results from the MAR model to the results of Moholdt et al.

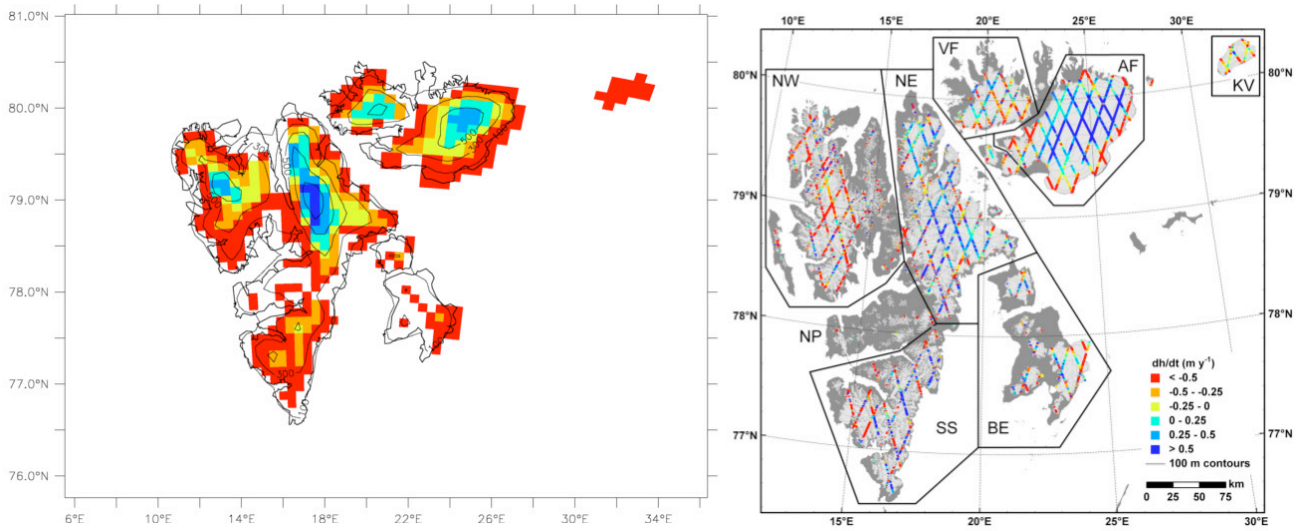

Figure 4.12: Mean annual elevation variation (m) for the 2003-2008 period calculated by the MAR model (left) and results from Moholdt et al. (right).

Figure 4.12 shows the same range of values for the mean annual elevation change calculated by the MAR model and Moholdt et al. However, as table 4.7 indicates, the mean annual elevation loss is too high for Svalbard in general and for each of the single zones. In particular, the model does not show SMB increase integrated over Austfonna (AF) and Northeastern Spitsbergen (NE) as it should.

Zone	**Moholdt et al.**	**MAR**
Austfonna	0.11±0.04	-0.40
Vestfonna	-0.16±0.08	-0.41
Northwestern Spitsbergen	-0.54±0.10	-0.58
Northeastern Spitsbergen	0.06±0.06	-0.36
Southern Spitsbergen	-0.15±0.16	-0.77
Barentsøya/Edgeøya	-0.17±0.11	-0.85
Kvitøya	-0.46±0.11	-0.61
Total Svalbard	-0.12±0.04	-0.52

Table 4.7: Comparison between mean annual elevation change (m y^{-1}) from 2003 to 2008 given by the MAR model and Moholdt et al. (2010).

There must thus be some pattern differences between the MAR model and reality. Indeed, on Northwestern Spitsbergen, we have less negative values at high altitude and we even have some accumulation on the highest tops, which Moholdt et al. hardly have. On Austfonna, we have, in a general way, too few accumulation at high altitude and too much loss at lower altitude, i.e. the MAR model simulates a lower surface mass balance

than in reality. On Northeastern Spitsbergen (NE), we have again too much elevation losses at low altitudes but the results match at higher altitudes, although the topography is poorly represented in this part of Svalbard. Moreover, we do not have the same trend when we look at the spatial differences between the model and the observations.

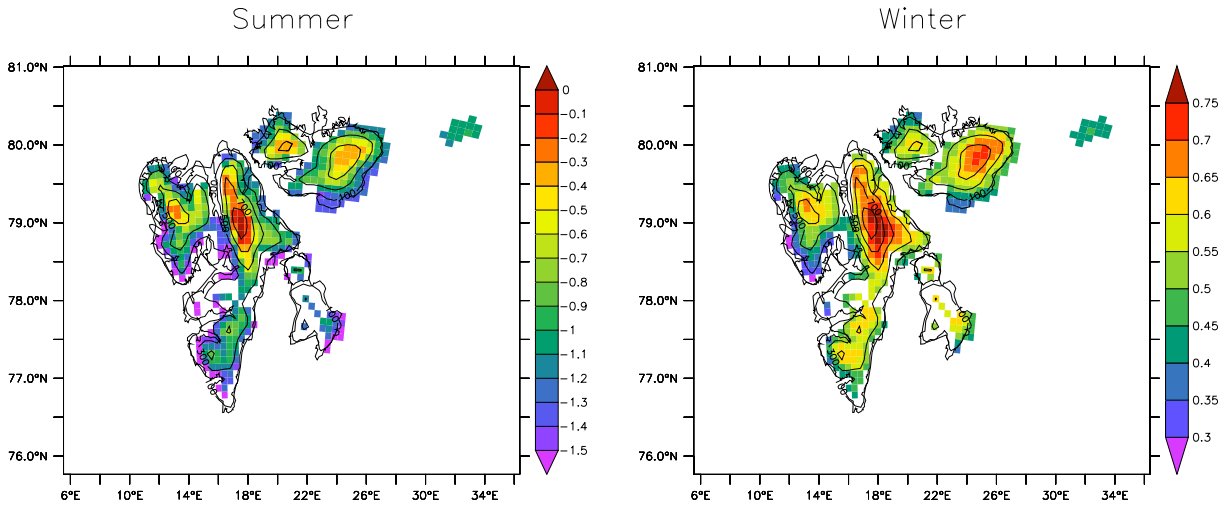

Figure 4.13: Mean summer (left) and winter (right) elevation variation (m) for the period 2003-2008. Summer balance is computed from March 2004 to October 2007 and winter balance from October 2003 to February 2008.

When we look at seasonal values, we see that the difference is mainly due to the higher melting in summer (see table 4.8), probably due to the lower topography. As for the total winter accumulation, the simulated values are much closer to those of Moholdt et al. Nevertheless, our values vary much less from one zone to another than the observed values does.

4.4 Conclusion

The mean annual surface mass balance modeled by the MAR model is negative at low altitudes and positive at higher altitude and the altitude where the balance is zero varies with the location. The values show a great interannual variability with a general decrease, which is not significant. The values are negative almost every year but could be underestimated due to an underestimation of the precipitation and an overestimation of the melting caused by the too low topography used in MAR.

The decrease of the surface mass balance is due to the increase of both runoff and precipitation. Mean summer temperature has also slightly increased over the last 53 years. However, none of these trends are significant.

The precipitation pattern follows the topography pattern but the simulated amount is underestimated. Runoff seems to be the major component of the surface mass balance as

	Summer		Winter	
	Moholdt et al.	**MAR**	**Moholdt et al.**	**MAR**
Austfonna	-0.40±0.08	-0.93	0.46±0.07	0.54
Vestfonna	-0.55±0.17	-0.87	0.30±0.13	0.50
Northwestern Spitsbergen	-1.09±0.16	-1.00	0.62±0.15	0.48
Northeastern Spitsbergen	-0.50±0.10	-0.87	0.61±0.10	0.60
Southern Spitsbergen	-0.87±0.23	-1.21	0.82±0.19	0.53
Barentsøya/Edgeøya	-1.02±0.29	-1.33	0.87±0.21	0.53
Kvitøya	-1.01±0.30	-1.05	0.42±0.25	0.44
Total Svalbard	-0.70±0.06	-1.00	0.60±0.05	0.54

Table 4.8: Comparison between seasonal elevation change (m y^{-1}) from given by the MAR model and Moholdt et al. (2010). Summer variations are computed from 15th February to 15th October in the MAR model and measured between February/March to October/November in Moholdt et al. from 2004 to 2007. Winter variations are computed from 15th October to 15th February in the MAR model and measured between October/November to February/March in Moholdt et al. from 2003/04 to 2007/08.

the mass balance spatial variability is inversely proportional to the runoff variability. The temperature pattern also reflects the topography variation but also present a longitudinal gradient due to the warmer waters brought by the North Atlantic Drift. Finally, the sublimation and evaporation gets smaller as the altitude increase. On the highest tops, its negative values are due to the higher deposition, itself due to a colder air.

Chapter 5

Results: correlations

This final chapter is going to investigate the correlation between the surface mass balance and its different components with the aim of finding which of those explain the surface mass balance variability. We are also going to see if the North Atlantic and Arctic Oscillations influence the surface mass balance in Svalbard or its components.

5.1 Correlations with the surface mass balance

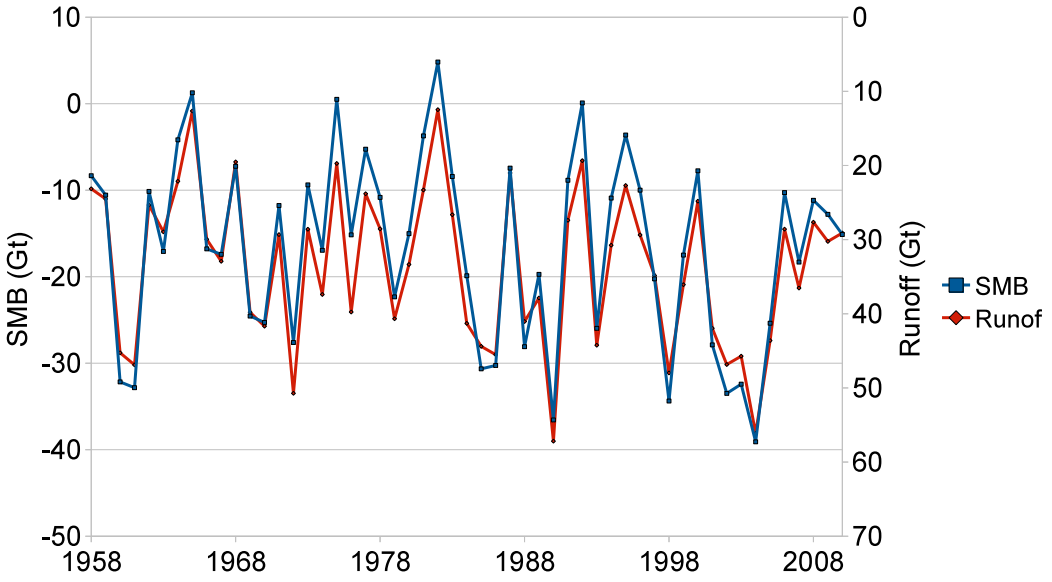

Figure 5.1: Evolution of the total annual surface mass balance (blue curve) and runoff (red curve) over 1958-2010. Runoff axis is reversed for clarity.

Figure 5.1 shows the evolution of the total annual surface mass balance (summed over

every pixel) together with the runoff from 1958 to 2010. The determination coefficient ($R^2 = 0.93$) indicates that the runoff mainly determines the interannual variations of the surface mass balance. Sublimation and evaporation do not count much in the total surface mass balance but the determination coefficient between the two series is 0.36. Finally, precipitation variability represents only 7 percent of the surface mass balance variability, as the amount of precipitation varies much less than the other terms of the surface mass balance and runoff and sublimation together represent the most part of the surface mass balance variability.

Variables		Correlation (R^2)
SMB	**Runoff**	0.93
	Precipitation	0.07
	Sublimation and evaporation	0.36
	Mean summer temperature	0.73
	Runoff and sublimation	0.95
Temperature	**Runoff**	0.84
	Sublimation	0.51
	Runoff and sublimation	0.82

Table 5.1: Summary of the correlations between SMB, its components and mean summer temperature.

Figure 5.2 shows the influence of the mean summer temperature (JJA) on the surface mass balance variability ($R^2 = 0.73$). The increase of the mean summer temperature is for the most part responsible for the acceleration of melt since 1958 due to its influence on the runoff ($R^2 = 0.84$ between mean summer temperature and runoff). However, as we have seen in chapter 4, temperature is not the only parameter influencing the amount of runoff. The amount of snowfall of the previous winter also impacts the appearance of bare ice zones where most of the runoff takes place the next summer. These low albedo zones are exposed once the winter snowpack has melted.

5.2 Correlation with the North Atlantic Oscillation and the Arctic oscillation

Finally, we have compared the variations of all the previous variables to the variability coming from the North Atlantic Oscillation (NAO) and the Arctic Oscillation (AO). The North Atlantic Oscillation index gives the anomaly of the pressure difference between the Icelandic Low and the Azores High with respect to the average value and influences, between others, the Northern Europe climate. If the NAO index is positive, the high pressure is stronger and the low is deeper than usual. This results in stronger westerlies bringing precipitation over Northern Europe and milder winters. If the index is negative, the high and the low are both weaker than usual, resulting in a lower pressure gradient

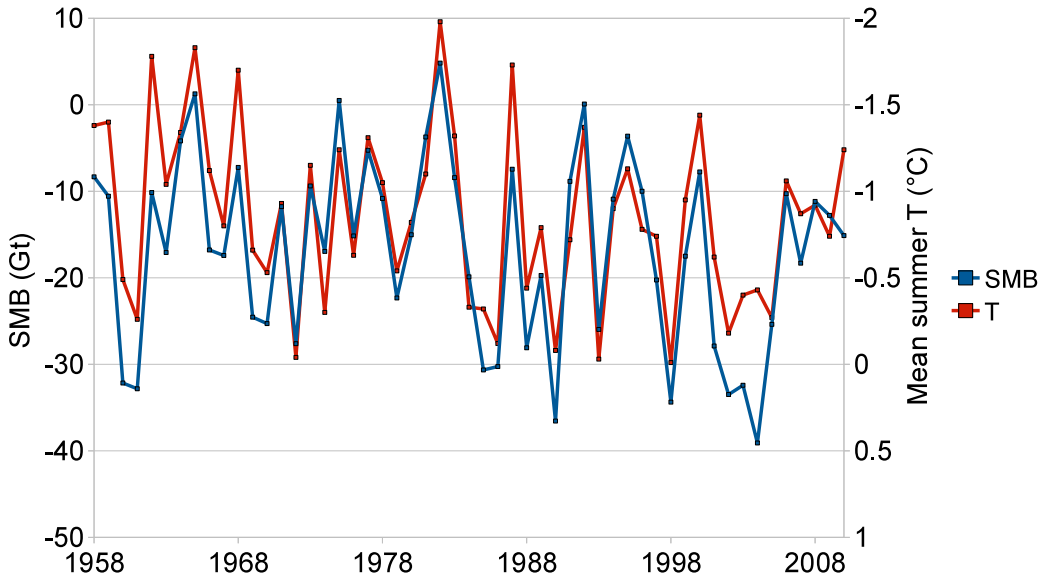

Figure 5.2: Evolution of the total annual surface mass balance (blue curve) and mean summer temperature (red curve) over 1958-2010. Temperature axis is reversed for clarity.

and thus, weaker westerlies. As a result, Northern Europe is influenced by cold arctic air and gets less precipitation.

According to the Climate Prediction Center of the NOAA (National Oceanic and Atmospheric Administration), "the daily AO index is constructed by projecting the daily (00Z) 1000mb height anomalies poleward of 20°N onto the loading pattern of the AO" and "the loading pattern of the AO is defined as the leading mode of Empirical Orthogonal Function (EOF) analysis of monthly mean 1000mb height during 1979-2000 period"[1]. Positive AO years are characterized by a sea level pressure lower than the normal. The resulting stronger Westerlies over North Atlantic prevent the arctic air from reaching mid-latitudes. The weather is thus again warmer and wetter than the normal in Northern Europe. Negative years, for their part, see a pressure pattern higher than normal in the Arctic. As a result, as in negative NAO years, Westerlies are weaker and cold dry polar air reaches more Southerly latitudes.

Neither or these two indexes' summer values explained the variations of the mean summer temperature and hence, the runoff or the surface mass balance (see table 5.2). Though, the variations of the annual value of the North Atlantic Oscillation explains 22 percent of the variability of the precipitation while the Arctic Oscillation explains 17 percent. Indeed, we can see in figure 5.3 that some of the positive NAO years have higher precipitation than the mean value (1964 for example) and some of the negative years have

[1]http://www.cpc.ncep.noaa.gov/products/precip/CWlink/daily_ao_index/ao_index.html

lower precipitation amount (1998). However, this is not significant.

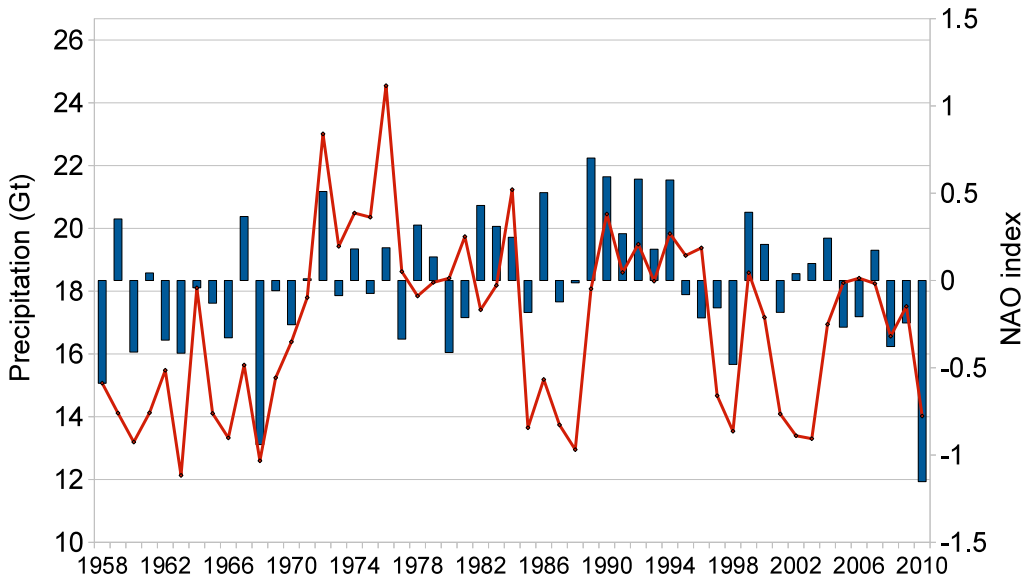

Figure 5.3: Evolution of the total annual amount of precipitation (red curve) and annual North oscillation Index (blue bars) over 1958-2010.

Variable		R^2 NAO	R^2 AO
Summer index (JJA)	**Temperature**	0.01	0.02
	Runoff	0.01	0.01
Annual index	**SMB**	0.00	0.00
	Precipitation	0.22	0.17

Table 5.2: Summary of the correlations between North Atlantic Oscillation and Arctic Oscillation indexes and mean summer temperature, runoff, surface mass balance and precipitation. Source of the indexes: www.cpc.ncep.noaa.gov

5.3 Conclusion

We have seen that the parameter that mostly determines the surface mass balance variability is the runoff, i.e. the melting variability induced in large part by the mean summer temperature variability. Sublimation and evaporation also explain a small fraction of the variability but precipitation, although counting for more than sublimation and evaporation in the total surface mass balance, does not explain much its variability. Finally,

neither the North Atlantic Oscillation nor the Arctic Oscillation influence the sign of the surface mass balance.

Chapter 6

Conclusion and perspectives

In this thesis, we have modeled the surface mass balance of the Svalbard cryosphere (ice caps and glaciers) with the MAR model forced by ECMWF reanalysis, its evolution from 1958 to 2010 and investigated its relation to its components and the climate.

The results show that the balance is negative at low altitude and positive at higher altitude, the equilibrium line altitude depending on the location in the archipelago. Precipitation and temperature patterns reflect the topography: the amount of precipitation rises with the altitude while the temperature drops. Moreover, we have shown the influence of the North Atlantic Drift on the temperature through its longitudinal gradient. The runoff pattern, for its part is inversely proportional to the surface mass balance pattern, the higher amount of runoff being found at lower altitude.

The surface mass balance evolution presents a general decrease from 1958 until now (but this trend is however not significant). The mean annual balance is also negative (-16.72 Gt yr^{-1}) and only some of the 53 modeled years show a positive balance. Runoff, precipitation and mean summer temperature have all increased over the 53 years but these trends are neither significant. Runoff variability is the main responsible for the surface mass balance variability ($R^2 = 0.93$) and is itself mainly determined by the mean summer temperature variability ($R^2 = 0.84$). Precipitation, although it is the main variable accounting for accumulation, varies much less and does not count much in the surface mass balance variability ($R^2 = 0.07$).

We have compared our results to those Moholdt et al. (2010) between 2003 and 2008. The modeled elevation change appears to be too negative and the difference is largely due to the higher modeled melting during the summer.

We have validated the model by comparing the modeled mean temperature, surface pressure, wind velocity and the total amount of precipitation to near-surface measurements coming from weather stations. The modeled temperature is well correlated to the observed values but the model is too cold by about 2 to 4 degrees. This will influence the surface mass balance through the temperature bias as well as its influence on the amount of precipitation. As for the mean seasonal temperature (summer and winter), the results indicated that the cold bias is reduced in summer, which will reduce the effect of temperature on the melting and increased in winter, which will reduce the amount of

precipitation but will increase the snowfall with respect to the liquid precipitation. Moreover, the modeled precipitation is not correlated to the observed amount and the total annual modeled amount is by far lower than the observations.

Other biases are also due to the bad topography produced by the GTOPO30 DEM. Indeed, the topography is generally too low, which underestimates the precipitation due to orographic lifting and overestimates the melting due to an overestimation of the temperature. Moreover, the 10-kilometer resolution is not able to represent the sharp topography of Spitsbergen. As a consequence, the numerous small glaciers found at higher altitude in these regions are represented at much lower altitude, which results in huge melting over these pixels that are not supposed to be covered with ice considering the altitude in our topography. Therefore, the model should be run at a higher resolution and with a better topography.

These runoff and precipitation biases might cause and underestimation of the surface mass balance of the Svalbard cryosphere.

Few long time series of surface mass balance are available as well as extensive measurements campaigns. However, polar regions are very sensitive to climate change. Therefore, regional climate model are well suited to evaluate the impacts of the global warming on the climate in general and on the cryosphere in particular, as well as modeling the current climate. In order to improve our results, we should though run the model with a higher resolution (5 kilometers for example) and use a more accurate topography. Moreover, more weather stations data are needed to validate the model over the current climate all over Svalbard. We should also test the integration domain size over more wet months to determine if we should increase its size or not.

Finally, in this thesis, we modeled only the surface mass balance but we could use the outputs of the MAR model to force an ice-sheet model, the SICOPOLIS (Simulation Code for Polythermal Ice Sheets) model for example, to include dynamical processes in our calculations (iceberg calving, basal melting,...). This would allow us to calculate the total mass balance over the Svalbard cryosphere and its contribution to sea level rise. Future projections could be made using GCM outputs from the CMIP5 data base, which will be used in the next IPCC report. Besides, in this thesis, the topography and ice mask were fixed. This was acceptable as we were only simulating present climate. With the coupling of the MAR model with an ice-sheet model, we could adjust the cryosphere topography every year, which is essential if we want to make future projections.

Appendix A

Linear regression equation

We would like to adjust an equation of the type A = a+b×t to the times series (A_i,t_i) where A_i is the value of the variable at the time t_i. The value of the parameters a and b is the value that allow χ^2 to be minimum.

$$\chi^2 = \sum_{i=1}^{N} \left(A_i - (a + b \times t_i)\right)^2$$

The minimum of χ^2 is obtained by calculating its derivatives with respect to both parameters.

We have thus

$$\begin{cases} \frac{\partial \chi^2}{\partial a} = 0 \\ \frac{\partial \chi^2}{\partial b} = 0 \end{cases} \iff \begin{cases} -2 \sum_{i=1}^{N} \left(A_i - a - b \times t_i\right) = 0 \\ -2 \sum_{i=1}^{N} t_i \left(A_i - a - b \times t_i\right) = 0 \end{cases}$$

$$\iff \begin{cases} \sum_{i=1}^{N} A_i - aN - b \sum_{i=1}^{N} t_i = 0 \\ \sum_{i=1}^{N} A_i t_i - a \sum_{i=1}^{N} t_i - b \sum_{i=1}^{N} t_i^2 = 0 \end{cases}$$

Let us put

$$\begin{cases} S_x = \sum_{i=1}^{N} t_i \\ S_y = \sum_{i=1}^{N} A_i \\ S_{xy} = \sum_{i=1}^{N} A_i t_i \\ S_{xx} = \sum_{i=1}^{N} t_i^2 \end{cases}$$

We have

$$\begin{cases} S_y - aN - bS_x = 0 \\ S_{xy} - aS_x - bS_{xx} = 0 \end{cases}$$

And the value of the parameters a and b is

$$\begin{cases} a = \dfrac{S_{xx}S_y - S_{xy}S_x}{\Delta} \\ b = \dfrac{NS_{xy} - S_xS_y}{\Delta} \end{cases}$$

with $\Delta = NS_{xx} - S_x^2$

Bibliography

[1] Bamber J.L., Krabill W., Raper V., Dowdeswell J.A., Oerlemans J. 2005. *Elevation changes measured on Svalbard glaciers and ice caps from airborne laser data*, Annals of Glaciology, 42, 202-208

[2] Dowdeswell J.A. 1986. *Drainage-basin characteristics of Nordaustlandet ice caps, Svalbard*, Journal of Glaciology, 32(110), 31-38

[3] Dowdeswell J.A., Drewry D.J., Cooper A.P.R, Gorman M.R., Listøl O., Orheim O. 1986. *Digital mapping of the Nordaustlandet ice caps from airborne geophysical investigations*, Annals of Glaciology, 8, 51-58

[4] Fettweis X. 2006. *Reconstruction of the 1979-2005 greenland ice sheet surface mass balance using satellite data and the regional climate model MAR*, PhD thesis, Université catholique de Louvain

[5] Fettweis X. 2007. *Reconstruction of the 1979–2006 Greenland ice sheet surface mass balance using the regional climate model MAR*, The Cryosphere, 1, 21-40

[6] Fettweis X., Tedesco M., van den Broeke M., Ettema J. 2011. *Melting trends over the Greenland ice sheet (1958-2009) from spaceborne microwave data and regional climate models*, The Cryosphere, 5, 359-375

[7] Fleming K.M., Dowdeswell J.A., Oerlemenas J. 1997. *Modelling the mass balance of northwest Spitsbergen glaciers and responses to climate change*, Annals of Glaciology, 24, 203-210

[8] Gallée H., Schayes G. 1994. *Development of a three-dimensional meso-γ primitive equation model: katabatic winds simulation in the area of Terra Nova Bay, Antarctica*, Monthly Weather Review, 122, 671-685

[9] Gallée H. 1995. *Simulation of the mesocyclonic activity in the Ross Sea, Antarctica*, Monthly Weather Review, 123, 2051-2069

[10] Gallée H., Pettré P., Schayes G. 1996. *Sudden cessation of katabatic winds in Adélie Land, Antarctica*, Journal of Applied Meteorology, 35,1142-1152

[11] De Ridder K., Gallée H. 1998. *Land Surface–Induced Regional Climate Change in Southern Israel*, Journal of Applied Meteorology, 37, 1470-1485

[12] Gallée H., Guyomarc'h G. Brun E. 2001. *Impact of snow drift on the Antarctic ice sheet surface mass balance: possible sensitivity to snow-surface properties*, Boundary-Layer Metorology, 99, 1-19

[13] Greuell W., Kohler J., Obleitner F., Glowacki P., Melvold K., Bernsen E., Oerlemans J. 2007. *Assessment of interannual variations in the surface mass balance of 18 Svalbard glaciers from the Moderate Resolution Imaging Spectroradiometer/Terra albedo product*, Journal of Geophysical Research, 112, D07105, doi:10.1029/2006JD007245

[14] Hagen J.O. 1988. *Glacier mass balance investigations in the balance year 1986-87*, Polar Research, 6, 205-209

[15] Hagen J.O., Liestøl O. 1990. *Long-term glacier mass-balance investigations in Svalbard*, 1950-88. Annals of Glaciology, 14, 102-106

[16] Hagen J.O., Lefauconnier B., Liestøl O. 1991. *Glacier mass-balance in Svalbard since 1912. Glaciers-Ocean-Atmosphere Interactions*. Proceedings of the Internationnal Symposium held at St Petersburg, September 1990. IAHS Publ. no. 208, 1991

[17] Hagen J.O. 1996. *Recent trends in the mass-balance of glaciers in Scandinavia and Svalbard*. Mem. Natl Inst. Polar Res., Spec. Issue, 51, 343-354, 1996

[18] Hagen J.O., Melvold K., Eiken T., Isaksson E., Lefauconnier B. 1999. *Mass-balance methods on Kongsvegen*, Svalbard Geographiska Annaler 81(A), 4, 593-601

[19] Hagen J.O., Kohler J., Melvold K., Winther J. 2003a. *Glaciers in Svalbard: mass balance, runoff and freshwater flux*, Polar Research 22(2), 145–159

[20] Hagen J.O., Melvold K., Pinglot J.F., Dowdeswell J.A. 2003b. *On the Net Mass Balance of the Glaciers and Ice Caps in Svalbard, Norwegian Arctic*, Arctic, Antarctic, and Alpine Research, 35(2), 264–270

[21] Hamilton G.S., Dowdeswell, J.A. 1996. *Controls on glacier surging in Svalbard, Journal of Glaciology*, 42 (140), 157-168

[22] Jiskoot H., Boyle P., T. Murray 1998. *The incidence of glacier surging in Svalbard: evidence from multivariate statistics*, Computers and Geosciences, 24(4), 387-399

[23] Lefauconnier B., Hagen J.O. 1990. *Glaciers and climate in Svalbard: statistical analysys and reconstruction of the Broggerbreen mass-balance for the last 77 years*. Annals of Glaciology, 14, 148-152

[24] Lefauconnier B., J. O. Hagen 1991. *Surging and calving glaciers in eastern Svalbard*, Norsk Polaarintitutt Meddelelser, 116

[25] Lefauconnier B., Hagen J.O., Pinglot J.F., Pourcher M. 1994. *Mass-balance estimates on the glacier complex Kongsvegen and Sveabreen, Spitsbergen, Svalbard, using radioactive layers*, Journal of Glaciology, 40(135), 368-376

[26] Liestol, O. 1993. *Glaciers of Europe - Glaciers of Svalbard, Norway. Chapter 5: Europe*, Satellite image atlas of glaciers of the world, edited by Williams R. S. and Ferrigno J.G., US Geological Survey professional paper, E127-E151

[27] Moholdt G., Hagen. J.O., Eiken T., Schuler T.V. 2009. *Geometric changes and mass balance of the Austfonna ice cap, Svalbard*, The Cryosphere Discussions, 3, 857–89

[28] Moholdt G., Nuth C., Hagen J.O., Kohler J. 2010. *Recent elevation changes of Svalbard glaciers derived from ICESat laser altimetry*, Remote Sensing of Environment, 114, 2756-2767, doi:10.1016/j.rse.2010.06.008

[29] Murray T, Strozzi T., Luckman A., Jiskoot H., Christakos P. 2003. *Is there a single mechanism? Contrasts in dynamics between glacier surges in Svalbard and other regions*, Journal of Geophysical Research, 108, B5, 2237, doi:10.1029/2002JB001906

[30] Nuth C., Moholdt G., Kohler J., Hagen J.O., Kääb A. 2010. *Svalbard glacier elevation changes and contribution to sea level rise*, Journal of Geophysical Research, 115, F01008, doi:10.1029/2008JF001223

[31] Pinglot J.F., Pourchet M., Lefauconnier B., Hagen J.O., Isaksson E., Vaikmäe R., Kamiyama K. 1999. *Accumulation in Svalbard glaciers deduced from ice cores with nuclear tests and Chernobyl reference layers*, Polar research, 18(2), 315-321

[32] Rasmussen L.A., Kohler J. 2007. *Mass-balance of three Svalbard glaciers reconstructed back to 1948*. Polar Research 26, 168-174

[33] Schuler T.V., Loe E., Taurisiano A., Eiken T., Hagen J.O., Kohler J. 2007. *Calibrating a surface mass-balance model for Austfonna ice cap, Svalbard*, Annals of Glaciology, 46, 241-248